Published in final edited form as:

J Comp Neurol. 2019 December 15; 527(18): 2948–2972. doi:10.1002/cne.24720.

Diverse spinal commissural neuron populations revealed by fate mapping and molecular profiling using a novel *Robo3*^{Cre} mouse

Alastair J. Tulloch[1,2,6], **Shaun Teo**[3,6,7], **Brigett V. Carvajal**[1,8], **Marc Tessier-Lavigne**[3,4], **Alexander Jaworski**[1,2,5]

[1]Department of Neuroscience, Brown University, Providence, RI

[2]Robert J. and Nancy D. Carney Institute for Brain Science, Providence, RI

[3]Laboratory of Brain Development and Repair, The Rockefeller University, New York, NY

[4]Department of Biology, Stanford University, Stanford, CA

Abstract

The two sides of the nervous system coordinate and integrate information via commissural neurons, which project axons across the midline. Commissural neurons in the spinal cord are a highly heterogeneous population of cells with respect to their birthplace, final cell body position, axonal trajectory, and neurotransmitter phenotype. Although commissural axon guidance during development has been studied in great detail, neither the developmental origins nor the mature phenotypes of commissural neurons have been characterized comprehensively, largely due to lack of selective genetic access to these neurons. Here, we generated mice expressing Cre recombinase from the *Robo3* locus specifically in commissural neurons. We used *Robo3*^{Cre} mice to characterize the transcriptome and various origins of developing commissural neurons, revealing new details about their extensive heterogeneity in molecular makeup and developmental lineage. Further, we followed the fate of commissural neurons into adulthood, thereby elucidating their settling positions and molecular diversity and providing evidence for possible functions in various spinal cord circuits. Our studies establish an important genetic entry point for further analyses of commissural neuron development, connectivity, and function.

Graphical Abstract

[5]Corresponding author: alexander_jaworski@brown.edu.
[7]Present address: Translational Research, Genome Institute of Singapore, Agency for Science, Technology and Research, Singapore
[8]Present address: Molecular Cardiology Research Institute, Tufts Medical Center, Boston, MA
[6]These authors contributed equally to this work.

DATA AVAILABILITY STATEMENT

The transcriptomic data that support the findings of this study are openly available in Figshare at http://doi.org/10.6084/m9.figshare.8023436.

COMPETING INTERESTS

No competing interests declared.

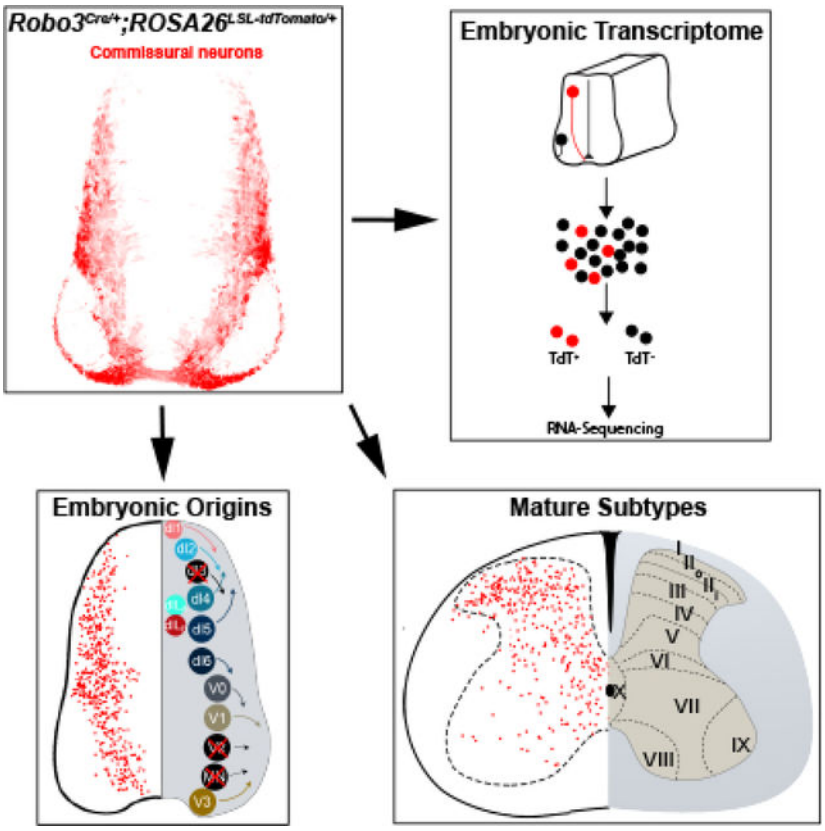

Robo3Cre mice provide genetic access to all commissural neurons in the spinal cord, revealing their diverse developmental origins and broad transcriptional, positional, and molecular heterogeneity.

Keywords

Commissural neurons; Robo3; spinal cord; neurogenesis; gene expression profiling; RRID: AB_10000320; RRID: AB_476667; RRID: AB_2278725; RRID: AB_528173; RRID: AB_531784; RRID: AB_2298772; RRID: AB_2314897; RRID: AB_2665452; RRID: AB_10000340; RRID: AB_2068524; RRID: AB_732428; RRID: AB_518504; RRID: AB_2565001; RRID: AB_632234; RRID: AB_2209751; RRID: AB_518614; RRID: AB_261562; RRID: AB_2532145; RRID: AB_2301751; RRID: AB_1587626; RRID: AB_2619825; RRID: AB_2135660; RRID: AB_2181865; RRID: AB_2044647; RRID: AB_2283049; RRID: AB_2155264; RRID: AB_2155412

1. INTRODUCTION

Despite its relative anatomical simplicity, the vertebrate spinal cord houses a large variety of neuronal subtypes. The extensive diversification of spinal cord neurons begins with their developmental origins. While patterning along the anterior-posterior axis generates functionally specialized spinal cord segments, the local organization of neurons at different rostro-caudal levels varies only modestly, and dorso-ventral patterning is the main driver of neuronal diversity in the developing spinal cord (Alaynick, Jessell, & Pfaff, 2011; Gouti,

Metzis, & Briscoe, 2015; Jessell, 2000; Lai, Seal, & Johnson, 2016). During the first wave of neurogenesis (embryonic day (E) 9.5-E12.5) in the mouse spinal cord, six dorsal (pd1-pd6) and five ventral progenitor zones (p0-p3 and pMN) generate eleven different populations of neurons (dI1-dI6, V0-V3, and motor neurons (MNs)), and two additional dorsal progenitor domains (pdL_A and pdL_B, giving rise to dIL_A and dIL_B neurons, respectively) contribute to the second wave of neurogenesis (E11-E13.5) (Helms & Johnson, 2003; Lai et al., 2016). Neurons originating from a common progenitor domain can frequently be subdivided further, such as V0 neurons (dorsal ($V0_D$), ventral ($V0_V$), and cholinergic/glutamatergic ($V0_{CG}$) subtypes) and V1 neurons (Renshaw cells ($V1_{Ren}$), inhibitory Ia interneurons ($V1_{IaIN}$), and the remaining V1 ($V1_{other}$) neurons). Different progenitor classes are defined by their combinatorial expression of transcription factors and their position along the dorso-ventral axis. In postmitotic neurons, expression of progenitor-specific patterning genes is extinguished and replaced by unique combinations of transcription factors that specify neuronal differentiation but are frequently not maintained into postnatal stages (Lai et al., 2016; Matise, 2013). Furthermore, the orderly arrangement of neuronal classes along the dorso-ventral axis becomes progressively muddled due to extensive cell migration and intermingling (Lai et al., 2016), such that the organization of the ten morphologically and functionally segregated laminae in the mature spinal cord (Rexed, 1952) does not correlate with the birthplace of the resident neurons. Together, these features of spinal cord development have complicated the task of elucidating connections between developmental classes and mature subtypes of neurons, as defined by their position, molecular makeup, connectivity, and function in different spinal cord circuits.

Interneurons and projection neurons in the spinal cord can be broadly subdivided into two categories depending on whether they innervate ipsi- or contralateral targets. Commissural (C-) neurons send axons across the floor plate (FP) at the spinal cord ventral midline and have served as a prime model system for studying mechanisms of axon guidance (Dickson & Zou, 2010; Martinez & Tran, 2015). The attractive guidance cues Netrin-1 and Sonic hedgehog (Shh), among other signals, promote C-axon growth to the FP (Charron, 2003; Kennedy, 1994). After midline crossing, C-axons are expelled from the FP and prevented from recrossing via FP-derived repellants of the Slit, Semaphorin, and Ephrin families (Kadison, Makinen, Klein, Henkemeyer, & Kaprielian, 2006; Parra & Zou, 2010; Zou, Stoeckli, Chen, & Tessier-Lavigne, 2000). The C- neuron-specific receptor Robo3 is a key regulator of precrossing C-axon guidance that promotes Netrin-1 signaling through the Netrin receptor DCC, prevents premature Slit repulsion through the Slit receptors Robo1 and Robo2, and mediates repulsion from its own ligand NELL2 in the spinal cord ventral horn (Jaworski et al., 2015; Sabatier, 2004; Zelina et al., 2014). These multiple activities of Robo3 are essential for midline crossing, as the ventral commissure fails to form and C-axons instead project through the ipsilateral ventral horn in mice lacking *Robo3* (Sabatier, 2004).

While C-neurons share some characteristics, including Robo3 expression, they are a highly heterogenous population of cells (Chedotal, 2014). Neuronal types as diverse as dI1 and V3 project axons across the midline (Alaynick et al., 2011; Lai et al., 2016), indicating that C-neurons arise from multiple progenitor domains in the developing dorsal and ventral neural tube. After midline crossing, C-axon trajectories diverge along the rostrocaudal axis, and

many rostrally-projecting axons ultimately innervate various supraspinal targets (Chedotal, 2014). Thus, different molecular programs must direct the integration of developing C-neuron subtypes into distinct neural circuits. In the adult spinal cord, C-neuron heterogeneity is apparent at the level of cell body position, neurotransmitter phenotype, connectivity, and function. Axonal tracing, electrophysiology, and spinal cord lesion studies have placed glycinergic, γ-aminobutyric acid (GABA)-ergic, and glutamatergic C-neurons in laminae I, III, IV, V, VI, VII, and VIII and demonstrated their participation in multiple critical circuit functions, such as local left-right coordination in the central pattern generator (CPG) and long-range nociceptive relay to the brain (Borowska et al., 2013; Chedotal, 2014; Eide, Glover, Kjaerulff, & Kiehn, 1999; Goulding, 2009; Goulding & Pfaff, 2005; Kiehn, 2011; Light, 1988; Petko, Veress, Vereb, Storm-Mathisen, & Antal, 2004; Restrepo et al., 2009; Stokke, Nissen, Glover, & Kiehn, 2002). Although the guidance of C- axons during development has been studied in great detail, neither the developmental origins nor the mature phenotypes of C-neurons have been characterized comprehensively. This is largely due to the extensive C-neuron heterogeneity and lack of a specific genetic marker that provides access to the entire population of neurons.

Here, we generated mice expressing Cre recombinase from the *Robo3* locus as a tool to label and manipulate C-neurons. While Robo3 is a highly specific marker for nascent C-axons, its protein expression is transient and largely excluded from cell bodies (Sabatier, 2004), but both of these limitations for labeling C-neurons are overcome by combining $Robo3^{Cre}$ mice with Cre-dependent fluorescent reporter lines. We used this approach to characterize the transcriptome of developing C-neurons and establish their molecular profile during development, thereby providing a valuable resource for investigation of genes involved in C-neuron development. Further, we elucidated the diverse developmental origins of C-neurons and quantified their distribution across different neuronal classes, revealing a substantial contribution of dI1 neurons to the C-neuron population during early neurogenesis, as well as a major combined contribution of dI4/dIL_A during both early and late waves of neurogenesis. Finally, we followed the fate of C-neurons in the adult spinal cord to quantitatively examine their position and molecular makeup. Our results show that C-neurons are found in regions that participate in processing various somatosensory modalities, exhibit broad molecular heterogeneity, and likely receive diverse presynaptic contacts, including direct inputs from sensory neurons. Together, our studies provide detailed insights into the development and ultimate fate of C-neurons, revealing extensive heterogeneity across multiple parameters. This quantitative stratification of C-neurons presents a key resource for interpreting bulk population studies of C-neuron development and for unraveling the relationship between developmental and functional C-neuron subtypes. Moreover, our $Robo3^{Cre}$ mice serve as an important genetic entry point for further analyses of C-neuron development, connectivity, and function.

2. MATERIALS AND METHODS

2.1 Animals

Mice carrying the conditional $Robo3^{cko}$ allele and the $ROSA26^{LSL\text{-}tdTomato}$ (Ai14) Cre-dependent reporter line have been described before and were genotyped as previously

reported (Madisen et al., 2010; Renier et al., 2010). For generation of the *Robo3*^{Cre} allele, a targeting construct was generated by a combination of gene synthesis (Blue Heron Biotechnology, Inc) and recombineering. The Cre coding sequence and a frt-flanked neomycin (Neo) cassette were inserted into exon 1 of the *Robo3* locus to replace the endogenous translation initiation codon and subsequent 31 nucleotides (Fig. 1a). The targeting vector was introduced into B6(Cg)-*Tyr*$^{C-2J}$/J mouse embryonic stem (ES) cells by standard procedures, and Neo-resistant colonies were screened by Southern blot analysis using probes upstream and downstream of the vector's homology arms. The ^{32}P-radiolabeled 5'- and 3'-probes were generated by PCR amplification from genomic DNA (primer sequences: 5' probe, CCACCTGGCCCTTGTTACCTC and CCTGATATTCCGTGGCTTAGTGTTG; 3'-probe, CTGCCTCTCCACCCCTTCACC and ATCCCCATCCCCACCAACATAGT) and use of the Prime-It II Random Primer Labeling Kit (Agilent). Correctly targeted ES cell clones were injected into B6 blastocysts to obtain chimeric mice following standard procedures at the The Rockefeller University Transgenic Services Laboratory. The Neo cassette was subsequently deleted to generate Robo3$^{Cre/+}$ mice by crossing the chimeras to *ACTB:FLPe B6J* mice, which express FLPe recombinase in the germ line (Rodriguez et al., 2000). For genotyping, the *Robo3*$^{+}$ and *Robo3*^{Cre} alleles were detected by PCR (primer sequences: ATCATAATCAGCCATACCACA, CTGCGCTACCTGCTTAAAACACTA, and CTGCCAGCGAGGAGTTGAAG) from genomic DNA, yielding band sizes of 112 and 355 base pairs (bps) for *Robo3*$^{+}$ and *Robo3*^{Cre}, respectively. Mice were maintained on a mixed background. While mice of either sex were used for all analyses, the *Robo3*^{Cre} allele was always contributed by the male parent when combining it with floxed alleles, as transmission through the female germline resulted in widespread, variable loxP recombination across tissues (data not shown), suggestive of unspecific Cre expression. All experimental procedures were approved by IACUCs at Brown University or The Rockefeller University and in compliance with National Institutes of Health guidelines.

2.2 Tissue dissociation and fluorescence-activated cell (FAC)-sorting of spinal cord cells expressing tdTomato

Between 3 and 4 E11.5 *Robo3*$^{Cre/+}$; *ROSA26*$^{LSL\text{-}tdTomato}$ spinal cords from the same litter (total of 3 separate litters) were dissected in the open-book configuration in ice-cold L-15 media (Gibco), and cut longitudinally into several smaller sections. The tissue from each individual litter was pooled, then digested with half a vial of papain (Worthington, PAP2) with 1mM $CaCl_2$, DNase (Worthington, D2) dissolved in 5 ml of HBSS-supplemented solution (HBSS (Gibco 14710), 0.3% glucose, 10 mM HEPES) at 37°C for 7 minutes (min), with gentle mixing. The supernatant was replaced by 5 ml of 2.5 mg/ml trypsin inhibitor (Sigma T6522) and 0.1% BSA in HBSS- supplemented solution. The suspension was triturated and filtered through a 70 μm nylon cell filter (Falcon), resuspended to 10^6 cells/ml in 0.1% BSA in Hank's balanced salt solution (HBSS)- supplemented solution on ice, and DAPI was added as a marker of cell death.

Cells were FAC-sorted using a BD FACSAria Cell Sorter system at The Rockefeller University Flow Cytometry Center. Sorting was gated according to tdTomato expression, and live cells were collected into separate vials (tdTomato-positive and -negative (tdT^{+} and

tdT^{-}) cells) containing lysis buffer from the RNeasy kit (Qiagen). RNA was extracted immediately using the RNeasy kit according to the manufacturer's instructions and stored at −80°C until library preparation. In total, 3 embryonic litters were used, resulting in 6 samples: 3 tdT^{+} RNA samples, and 3 tdT^{-} RNA samples.

2.3 RNA library preparation

All RNA samples were verified on a Bioanalyzer Picochip, and had an RNA integrity number of over 8.5 (Agilent). 100 ng total RNA of each of the 6 samples was used as input material for cDNA library preparation using TruSeq RNA Sample Prep Kit v2 (Illumina). The 6 libraries were prepared simultaneously to minimize batch variation. Libraries were multiplexed and sequenced on a HiSeq 2500 (Illumina) at the Genomics Resource Center at The Rockefeller University to generate 30×10^6 of single-end 100-bp reads per library.

2.4 RNA-Seq alignment and analysis

RNA-Seq reads were aligned to the GRCm38 (mm10) Reference genome. Read alignment, transcriptome alignment, and differential analysis were done using the Tuxedo protocol as published (Trapnell et al., 2012). Using default parameters, the false discovery rate (FDR) is 0.05, and genes were considered significantly enriched if the FDR-adjusted *p*-value (i.e. *q*-value) is lower than 0.05. The RNA-Seq expression-enrichment plots were explored and graphed in R (R.- Core-Team, 2017). Mouse (Organism: 10090) genes annotated as encoding cell membrane proteins (gene ontology (GO) term analysis "cell membrane", number: 05886; downloaded 28 July 2018) were obtained from the UniProt website (The UniProt Consortium, 2017).

2.5 *In situ* hybridization

To generate *in situ* hybridization probes, we obtained cDNA library clones of target genes (Dharmacon). Target sequences were PCR-amplified using gene-specific primer sequences (Table 1) with T7 and T3 promoters incorporated into the 5' ends of the forward and reverse primer, respectively. The T7 and T3 promoters were then used to generate Digoxigenin-11-D- UTP (DIG)-labeled probes by *in vitro* transcription with DIG RNA labeling mix (Roche).

Fluorescence *in situ* hybridization was performed using embryos immersion-fixed for 30 min in 4% paraformaldehyde (PFA) and phosphate-buffered saline (PBS) at room temperature (RT), and cryoprotected with 10% sucrose in PBS overnight (O/N) at 4°C. Embryos were embedded in gelatin-sucrose, frozen, and forelimb-level transverse spinal cords were cryosectioned onto slides at 14 μm. Tissue sections were post-fixed for 10 min with 4% PFA in PBS, rinsed three times in PBS, then acetylated for 8 min. The tissues were rinsed for 30 min in 0.5% Triton X-100 in PBS, followed by 3 rinses in PBS. Sections were pre-hybridized for 2 hours (h) at RT in hybridization solution (50% formamide, 5X SSC, 5X Denhardt's solution, 0.5 mg/mL salmon testes DNA, 0.24 mg/mL baker's yeast tRNA), and subsequently incubated with a coverslip with DIG-labeled riboprobe in hybridization solution O/N at 72°C in a humidifying chamber. The following day, sections were dipped into a 5X SSC solution at 72°C, and incubated in 0.2X SSC at 72°C for 90 min. The sections were cooled to room temperature and blocked with TNB solution (0.5% TSA blocking reagent (PerkinElmer), 100mM Tris/HCl pH 7.6, 0.15 M NaCl). Sections were incubated for

1 h with 1:500 anti-DIG HRP antibody (Roche) in TNB. Sections were washed five times with TNT buffer (0.1% Tween-20, 100 mM Tris/HCl pH 7.6, 0.15 M NaCl). DIG signal on sections was amplified using the TSA Cy3 system for 10 min exactly according to manufacturer's instructions. The reaction was quenched using 1% NaN_3 in TNT buffer for 10 min, then washed five times for 5 min in TNT buffer. For immunofluorescent detection of tdTomato following hybridization, sections were first blocked in 3% donkey serum and 0.1% Triton X-100 in PBS, and then incubated with a polyclonal rabbit antibody against Red Fluorescent Protein (RFP) (1:1000, Rockland Immunochemicals) in blocking solution O/N at 4°C. Sections were washed with 0.1% Triton X-100 in PBS, incubated with an Alexa488-conjugated donkey secondary antibody (1:500–1:1000, Invitrogen) for 1 h. The slides were then washed in 0.1% Triton X-100 in PBS, mounted under Fluoromount G (Electron Microscopy Sciences), and microscope images were pseudo-colored after acquisition.

2.6 Immunohistochemistry

Unless indicated otherwise, all incubations were performed at RT. Mouse embryos were immersion-fixed in 4% PFA in PBS O/N at 4°C. Adult mice were perfusion-fixed with 4% PFA in PBS and harvested brachial spinal cords were immersion-fixed O/N at 4°C. Following three 1-h rinses in PBS, tissues were incubated in 30% sucrose and PBS for 24–48 h at 4°C, and embedded in OCT. Transverse cryostat sections (20 μm) were incubated in 10 mM sodium citrate and 0.05% Tween-20 in PBS for 20 min at 85°C, rinsed two times for 5 min in PBS, and blocked in either 2.5% normal goat serum or 2.5% bovine serum albumin and 0.1% Tween-20 (0.2% Triton X-100 for adult tissue) in PBS for 1 h (O/N for adult tissues). Tissues were incubated with primary antibodies O/N at 4°C (48 h for adult tissues) and with secondary antibodies for 1 h at RT (3 h for adult tissues) in blocking solution, rinsed three times with 0.1% Tween-20 (0.2% Triton X-100 for adult tissue) in PBS between and after antibody incubations, and mounted using Fluoromount G. Sequential incubations with primary and secondary antibody pairs were performed when mouse and rat primary antibodies needed to be combined onto the same slide; following the first primary and secondary antibody incubations, tissues were treated with unconjugated donkey anti-mouse FAB fragments (20 μg/ml, Jackson Immunoresearch #715-007-003) to block double labeling of primary antibodies.

2.7 Antibody Characterization

Mouse monoclonal antibodies raised against Barhl2 (1:100, Novus #NBP2–32013), Calretinin (CR) (1:1000, Swant #6B3), GABA (1:200, Sigma-Aldrich #A0310), glutamic acid decarboxylase (GAD)67 (1:500, Millipore #MAB5406), Isl1/2 (1:200, DSHB #39.4D5), LIM homeobox (Lhx)-1/5 (1:200, DSHB #4F2), NeuN (1:100, Millipore #MAB377), and neurofilament (NF) (1:1000, DSHB #2H3), as well as a rat polyclonal antibody raised against Bhlhb5 (1:5000, Sarah Ross (Ross et al., 2010), University of Pittsburgh, Pittsburgh PA) were used. The antibody against recombinant Barhl2 protein was validated using a protein array and used in previous reports (Junge, Yung, Goodrich, & Chen, 2016; Leggere et al., 2016). The anti-CR antibody (RRID: AB_10000320) recognizes an epitope within the first 4 EF-hands domains common to both calretinin and calretinin-22k, and stains a band corresponding to the molecular weight of calretinin in western blot of brain extracts from various vertebrate species (Zimmermann & Schwaller,

2002). The anti-GABA antibody (RRID: AB_476667) was derived from the hybridoma produced by the fusion of mouse myeloma cells and splenocytes. It was generated against GABA conjugated to bovine serum albumin and was validated using a dot blot immunoassay, which showed weak cross-reaction with β-alanine and ε-aminocaproic acid. The anti-GAD67 antibody (RRID: AB_2278725) was derived from recombinant GAD67 protein and validated by Western blot (67kDa) (Erlander, Tillakaratne, Feldblum, Patel, & Tobin, 1991) and *GAD67* conditional knockout mutants (Heusner, Beutler, Houser, & Palmiter, 2008). The anti-Isl1/2 antibody (RRID: AB_528173) was raised against the C-terminal portion of rat Islet 1 (aa 178–349) and was validated by comparison of the labeling patterns obtained by immunohistochemistry (IHC) and by in situ hybridization (Tsuchida et al., 1994). The anti-Lhx1/5 antibody raised against recombinant rat Lim2 (RRID: AB_531784) detects both Lim1 and Lim2 and was validated by *in situ* hybridization and immunostaining (Tsuchida et al., 1994). The anti-NeuN antibody (RRID: AB_2298772) was raised against purified cell nuclei from mouse brain and was validated by western blot and immunostaining of various species (Mullen, Buck, & Smith, 1992). The anti-NF antibody (RRID: AB_2314897) was raised against a membrane preparation obtained from E14–E15 rat spinal cord tissue and was validated by western blot (155–165 kDa) from PC12 cells and spinal cord tissue (Dodd, Morton, Karagogeos, Yamamoto, & Jessell, 1988). The anti-Bhlhb5 antibody (RRID: AB_2665452) was raised against GST-fusion proteins encompassing either an N-terminal or C-terminal epitope of Bhlhb5 and was validated using Bhlhb5 knockout mutants (Ross et al., 2010).

Rabbit polyclonal antibodies raised against Calbindin D-28k (CB) (1:1000, Swant #CB38), calcitonin gene-related protein (CGRP) (1:250, Calbiochem #PC205L), Foxp1 (1:1000, Abcam #ab16645), NPY (1:250 Peninsula Laboratories #T-4070), Pax2 (1:200, Biolegend #901001), protein kinase C (PKC)-γ (1:250, Santa Cruz #sc-211), RFP (1:500, Rockland #600-401-379), Somatostatin (Sst) (1:1000, Peninsula Laboratories #T-4103), and Substance P (neurokinin-1) receptor (NK-1R) (1:200, Sigma-Aldrich #s8305) were used. The anti-CB antibody (RRID: AB_10000340) was validated by western blot and CB knockout mutants (Airaksinen et al., 1997). The antibody raised against rat α-CGRP (RRID: AB_2068524) showed a pattern and distribution consistent with other IHC stains in the developing spinal cord (Harmann, Chung, Briner, Westlund, & Carlton, 1988). The anti-Foxp1 antibody (RRID: AB_732428) was raised against a synthetic C- terminus peptide of Human FOXP1 conjugated to KLH and showed a pattern and distribution consistent with previous spinal cord staining (Rousso, Gaber, Wellik, Morrisey, & Novitch, 2008). The anti-NPY antibody (RRID: AB_518504) was raised against rat NPY and validated by radioimmunoassays and with a pattern and distribution consistent with previous spinal cord staining (Polgar, Sardella, Watanabe, & Todd, 2011). The anti-Pax2 antibody (RRID: AB_2565001) was raised against a recombinant protein containing 22kD of the Pax2 sequence and was validated by western blot (Dressler & Douglass, 1992). The anti-PKC-γ antibody (RRID: AB_632234) was raised against a C-terminus peptide of mouse PKC-γ and validated by western blot and shows a pattern and distribution consistent with previous spinal cord staining (H. Y. Huang et al., 2005). The anti-RFP antibody (RRID: AB_2209751) was raised against mushroom polyp coral Discosoma and validated by western blot, reflecting a pattern and distribution consistent with endogenous tdTomato fluorescence (Fig. 1). Anti-Sst

antibody (RRID: AB_518614) was raised against an N-terminus synthetic peptide and validated using a Sst knockout mutant (Saito et al., 2005). The anti-NK-1R antibody (RRID: AB_261562) was raised against a rat C-terminus synthetic peptide and was validated using a NK-1R knockout mutant (Ptak et al., 2002).

Guinea pig polyclonal antibodies raised against GlyT2 (1:500, Synaptic Systems #272 004), Tlx-3 (1:10,000, Carmen Birchmeier (Storm et al., 2009), Max-Delbrück-Centrum for Molecular Medicine, Berlin), vesicular glutamate transporter (vGluT)-1 (1:200, Millipore #AB5905), vGluT2 (1:200, Millipore #AB2251), and vGluT3 (1:500, Synaptic Systems #135 204) were also used. The anti-GlyT2 antibody was raised against a rat N-terminus 229-AA peptide and validated by western blot, reflecting a pattern and distribution consistent with previous spinal cord staining (Corleto et al., 2015). The anti-Tlx-3 antibody (RRID: AB_2532145) was raised against a His-tagged recombinant Tlx-3 protein and exhibits a staining pattern in the spinal cord consistent with a Lacz reporter driven by *Tlx-3*^{Cre} (Xu et al., 2008). The anti-vGluT1 antibody (RRID: AB_2301751) was raised against the C-terminus of rat vGlut1 and was validated by western blot (Melone, Burette, & Weinberg, 2005). The anti-vGluT2 antibody (RRID: AB_1587626) was raised against a GST tagged Recombinant protein and validated by western blot (Montana, Ni, Sunjara, Hua, & Parpura, 2004). The anti-vGluT3 antibody (RRID: AB_2619825) was raised against a mouse recombinant peptide and validated by vGluT3 knockout mutants (Fasano et al., 2017).

Goat polyclonal antibodies raised against Lhx2 (1:200, Santa Cruz #sc-19344), Robo3 (1:200, R&D Systems #AF3076), transient axonal glycoprotein (TAG)-1 (1:200, R&D Systems #AF4439), tropomyosin receptor kinase (Trk)-A (1:200, R&D Systems #AF1056), TrkB (1:50, R&D Systems #AF1494), and TrkC (1:40, R&D Systems #AF1404) were used. The anti-Lhx2 antibody (RRID: AB_2135660) was raised against a C-terminus peptide of Lhx2 of human origin and has been used to specifically label Lhx2-positive dI1 neurons in the developing spinal cord (Kaneyama & Shirasaki, 2018). The anti-Robo3 antibody (RRID: AB_2181865) was raised against the extracellular domain of recombinant human Robo3 and validated by Robo3 conditional knockout mutants (Fig. 1). The anti-TAG-1 antibody (RRID: AB_2044647) was raised against a recombinant mouse Contactin-2/TAG-1 protein and validated by a consistent pattern and distribution of other spinal cord staining (Sabatier, 2004). The anti-TrkA antibody (RRID: AB_2283049) was raised against mouse myeloma cell line NS0-derived recombinant rat TrkA (Ala33-Pro418) and validated by ELISA and western blot, showing a pattern and distribution consistent with previous spinal cord staining (Averill, McMahon, Clary, Reichardt, & Priestley, 1995). The anti-TrkB antibody (RRID: AB_2155264) was raised against mouse myeloma cell line NS0-derived recombinant mouse TrkB (Cys32-His429) and validated by ELISA and western blot, showing a pattern and distribution consistent with previous spinal cord staining (Macias et al., 2007). The anti-TrkC antibody (RRID: AB_2155412) was raised against mouse myeloma cell line NS0-derived recombinant mouse TrkC (Cys32-Thr429) and validated by ELISA and western blot, showing a pattern and distribution consistent with previous spinal cord staining (Genc, Ozdinler, Mendoza, & Erzurumlu, 2004).

The following fluorescent markers were included during the secondary antibody incubation step: Isolectin B4 (IB4) from *Griffonia simplicifolia* conjugated to Alexa647 (1:100,

Invitrogen I32450) and Hoechst 33342 (1:1000, Life Technologies #H3570). Alexa405-, Alexa488-, Alexa594-, and Alexa647-conjugated secondary antibodies (1:200; Jackson ImmunoResearch Lab or Molecular Probes) raised in donkey or goat against respective primary antibody species were also used.

2.8 DiO tracing

Following fixation as described for IHC, embryonic and adult spinal cords (n=3 per age) were sectioned using a vibratome at 150 μm and injected with DiO (Thermo Fisher, #V22886) in locations indicated in figure legends. Embryonic sections were mounted under Fluoromount G ~48 h post-injection and imaged immediately. Adult sections were mounted ~48 h post-injection and imaged 120–168 h post-injection.

2.9 Image Acquisition and processing/analysis

Embryonic and adult spinal cord sections were imaged with either a Zeiss LSM 800 Axio Imager Z2 confocal laser scanning microscope, a Nikon Eclipse 90i coupled to a Nikon QiMc camera, or with a Nikon Eclipse Ti inverted fluorescent microscope with an Andor CCD camera. Images were processed and analyzed using either NIS-Elements software (Nikon Instruments Inc.) or ImageJ. Cell body distribution plots were generated in Python after performing an affine transform of all images and cell position coordinates using ImageJ in order to standardize the spinal cord morphology across multiple sections and animals. Coordinates for tdT^+ cell bodies from three mice (three sections per animal) at each age were transformed and plotted on a standardized outline of a spinal cord and randomly down-sampled to reflect the distribution of cell bodies in a single spinal cord section.

2.10 Experimental Design and Statistical Analysis

A minimum of three mice (n) were analyzed for all descriptive statistics (n is indicated in figure legends), and the number of quantified spinal cord hemisections per n ranged from 4–54. For all descriptive statistics, the quantified hemisections within each animal (i.e., technical replicates) were averaged, generating a single mean value per n; the averages and SEMs of the biological replicates were subsequently calculated and displayed.

To quantify the number of DiO^+ cells in embryonic and adult tissues, either single focal planes (for embryonic analysis due to the high density of cells) or maximum projections from ~50–100 μm (for adult analysis) were used. The ImageJ plugin Cell Counter was used to count the number of cells that were labeled with either or both tdTomato and DiO (E11.5 and adult ages), and with tdTomato and/or a combination of IHC markers (all embryonic ages).

Embryonic neuronal subtype analysis.—Combinations of markers and position were used to identify the post-mitotic neurons that arise from different progenitor domains (Alaynick et al., 2011; Lai et al., 2016) (see Table 2) in $Robo3^{Cre/+};ROSA26^{LSL\text{-}tdTomato/+}$ mice (n=3 animals; 3 sections per n; quantified by hemisection). Progenitor domains were identified by the following transcription factor expression profiles and (if needed) positional criteria: dI1 – Barhl2 and/or Lhx2 (Fig. 6d); dI2 – $Lhx1/5^+/Pax2^-$ staining at E10.5 and E11.5 (Fig. 6e), $Foxp1^+$ staining dorsal of the motor columns at E12.5 and E14.5 (images

not shown; this is a subset of dI2, and FoxP1 was used because Lhx1/5 staining becomes extremely weak after E11.5); dI3 – $Isl1/2^{+}/Tlx3^{+}$ staining (Fig. 6f); $dI4/dIL_{A}$ – $Pax2^{+}/Lhx1/5^{+}$ staining at E10.5 and E11.5 (Fig. 6e), $Pax2^{+}$ dorsal cluster (due to loss of Lhx1/5 staining), clearly separated from ventral (dI6) cluster at E12.5 and E14.5 (Fig. 6g); $dI5/dIL_{B}$ – $Tlx3^{+}/Isl1/2^{-}$ staining (Fig. 6f); dI6 and $V1_{Ren/IaIN}$ – $Lhx1/5^{+}/Bhlhb5^{+}/Foxp1^{-}$ staining, with sufficient dorso-ventral separation between the two populations at E10.5 to identify distinctly (Fig. 6h); V0 – $Lhx1/5^{+}/Bhlhb5^{-}/Foxp1^{-}$ cluster, clearly separated from dorsal dI2/dI4 cluster (Fig. 6h); $V1_{other}$ – $Lhx1/5^{+}/Bhlhb5^{+}/Foxp1^{+}$ staining (Fig. 6h); V2 – $Lhx1/5^{-}/Bhlhb5^{+}/Foxp1^{-}$ staining (Fig. 6h).

Adult analysis.—To characterize the positions of C-neurons in adult spinal cords, NIS Elements software was used to create ROIs based on the intensity of a fluorescent label that marks one or several laminae, and a spot detection tool was used to identify tdT^{+} cells both within and outside of the marked lamina(e). To characterize neuronal subtypes of C-neurons, the spot detection tool was used to identify cells positive for neuronal subtype markers or tdTomato and the extent of their co-localization. To determine the fraction of C-neurons in each lamina (n=5 animals; ≥ 4 sections per n; quantified by hemisection), either individual ROIs were used (laminae I, II_{outer}, and II_{inner}), or a subtractive strategy (III-X) that was applied to combinations of ROIs (Fig. 9a–b). TdT^{+} neurons residing within intensity-defined ROIs were quantified using the NIS Elements software – lamina(e): I (NK-1R); II_{outer} (IB4); II_{inner} (PKC-γ); III (CB – [I + II_{outer} + II_{inner}]); IV-X (all C-neurons – [I + II_{outer} + II_{inner} + III]) (Todd, 2010). C-neurons co-labeled with a neuronal marker were also quantified (n=3 animals; ≥4 sections per n; quantified by hemisection), according to the fraction of C-neurons within a particular subtype, or the contribution of the neuronal subtype to the C-neuron pool (Fig. 11a–h).

3. RESULTS

3.1 A *Robo3^{Cre}* allele drives Cre-mediated recombination in embryonic spinal commissural neurons.

Robo3 is an axon guidance receptor exclusively expressed by C-neurons in the developing embryonic spinal cord, and it is required for C-axons to cross the ventral midline (Sabatier, 2004). To gain genetic access to spinal C-neurons, we generated a knock-in mouse that expresses Cre recombinase from the *Robo3* locus (Fig. 1a). The *Cre* coding sequence, followed by a frt-flanked neomycin selection cassette, was inserted into *Robo3* exon 1 through homologous recombination in ES cells, and correct targeting was confirmed by Southern blot (Fig. 1b). In mice generated from positive ES cell clones, the neomycin cassette was subsequently removed (Fig. 1a, see Materials and Methods). To examine the relationship between Cre activity and Robo3 expression in the resulting *Robo3^{Cre}* mice, we crossed them to the *ROSA26$^{LSL\text{-}tdTomato}$* reporter line that expresses the RFP variant tdTomato in a Cre-dependent manner (Madisen et al., 2010). We performed Robo3 and RFP immunostaining of E9.75, E10.5, and E11.5 brachial spinal cord transverse sections from *Robo3$^{Cre/+}$; ROSA26$^{LSL\text{-}tdTomato/+}$* mice and found that tdTomato immunoreactivity faithfully labels Robo3-positive neurons and their axons (Fig. 1c). At E9.75, the first few postmitotic C-neurons start expressing Robo3 and project short axons towards the FP, and

these cells are labeled by the RFP antibody (Fig. 1c, top row), indicating that there is little or no temporal delay between Robo3 and tdTomato expression in C-neurons. At E10.5 and E11.5, when increasing numbers of C-neurons send axons across the midline, Robo3 expression appears much stronger on axons than on cell bodies, while tdTomato staining continues to strongly label both somata and axons (Fig. 1c, middle and bottom rows); moreover, Robo3 protein on C-axons is down-regulated after midline crossing (Chen, Gore, Long, Ma, & Tessier-Lavigne, 2008), but postcrossing axons exhibit clear tdTomato immunoreactivity (Fig. 1c, column 2). Importantly, no tdTomato staining was observed in spinal cords of $ROSA26^{LSL\text{-}tdTomato/+}$ mice (data not shown) or in Robo3-negative cells of $Robo3^{Cre/+}; ROSA26^{LSL\text{-}tdTomato/+}$ embryos (Fig. 1c), indicating that labeling is strictly dependent on Cre activity in Robo3-expressing cells. Although weaker in intensity, endogenous tdTomato fluorescence mirrors the pattern of tdTomato immunoreactivity (Fig. 1c, columns 2 and 3), and it aligns closely with the precrossing C-axon marker TAG-1 but not panaxonal NF staining, as shown by antibody labeling in E11.5 spinal cord (Fig. 1d). Together, these data demonstrate that tdTomato faithfully labels all and only Robo3- positive cells in $Robo3^{Cre/+}; ROSA26^{LSL\text{-}tdTomato/+}$ embryonic spinal cord and support the idea that the $Robo3^{Cre}$ line specifically deletes floxed alleles in C-neurons.

To confirm that $Robo3^{Cre}$ targets all C-neurons, we crossed $Robo3^{Cre/+}$ mice with mice carrying a conditional *Robo3* knock-out allele ($Robo3^{cko}$)(Renier et al., 2010) and analyzed their offspring by staining E11.5 brachial spinal cord transverse sections with antibodies against NF and Robo3 (Fig. 2a). $Robo3^{Cre}$ is itself a null allele for *Robo3*, as $Robo3^{Cre/-}$ mice phenocopy the lack of C-axon midline crossing observed in $Robo3^{-/-}$ mice (data not shown). Similarly, the ventral commissure is completely absent in E11.5 $Robo3^{Cre/cko}$ embryos, and Robo3 immunoreactivity is efficiently abolished, while $Robo3^{cko/+}$ littermates exhibit normal midline crossing and Robo3 expression (Fig. 2a). These data indicate that $Robo3^{Cre}$ deletes the floxed $Robo3^{cko}$ allele in all C-neurons. To further test whether $Robo3^{Cre}$ drives Cre activity in all C-neurons, we performed retrograde tracing experiments in $Robo3^{Cre/+}; ROSA26^{LSL\text{-}tdTomato/+}$ embryos (Fig. 2b). We unilaterally injected the lipophilic dye DiO into the ventrolateral funiculus adjacent to the ventral commissure in E11.5 brachial spinal cord and found that 100% of DiO-positive neuronal cell bodies contralateral to the injection site also express tdTomato (Fig. 2b, top row), confirming Cre-mediated recombination in all C-neurons. DiO labeling efficiency in these experiments is 30.7±3.81% of contralateral tdT^+ cells, leaving the theoretical possibility that some tdT^+ cells project ipsilaterally. To address this caveat, we performed DiO injections in the ventrolateral funiculus further away from the midline, where many ipsilaterally projecting axons join the fiber tracts. We examined retrogradely traced neurons ipsilateral to the injection site and found that this labeling paradigm exclusively captures tdT^- cells (Fig. 2b, bottom row), arguing against ipsilateral projections of tdT^+ cells into the injection site. Thus, $Robo3^{Cre}$ effectively and specifically drives Cre activity in C-neurons of the developing spinal cord.

3.2 Transcriptomic analysis of embryonic commissural neurons identifies preferentially expressed genes and reveals molecular heterogeneity.

To characterize the molecular makeup of embryonic C-neurons, we analyzed their transcriptome by sorting spinal cord neurons from E11.5 *Robo3*$^{Cre/+}$; *ROSA26*$^{LSL\text{-}tdTomato/+}$ embryos based on their tdTomato fluorescence and performing RNA-Seq analysis (Fig. 3a). After FAC-sorting of tdT^{+} and tdT^{-} populations (Fig. 3b, **top panel**), isolated tdT^{+} cells accounted for approximately 8% of all sorted cells (Fig. 3b, **bottom panel**). Due to the stringent gating criteria for defining tdT^{+} cells, this is likely a lower bound estimate for the fraction of cells in the spinal cord that are C-neurons. RNA-Seq analysis of the tdT^{+} and tdT^{-} populations revealed 2,908 mRNAs that are significantly enriched in C-neurons (Fig. 3c, Table S1, see Materials and Methods for cutoff criteria). 620 of the enriched transcripts fall into the gene ontology (GO) term analysis group “cell membrane” (Fig. 3c, Table S1). This includes the Robo family members *Robo1* and *Robo3*, which were enriched 2.66- and 16.42-fold, respectively, while *Robo2* expression levels in the two populations were indistinguishable (Fig. 3d). The low level of *Robo3* in tdT^{-} cells likely results from the stringent gating for sorting of the tdT^{+} population, and this effect may be compounded by a slight delay between *Robo3* mRNA and tdTomato protein expression. We compared expression levels of other known guidance cue receptors that mediate axon repulsion (Fig. 3e). We found that multiple Semaphorin receptors are significantly enriched in C-neurons – this includes *Nrp2*, *Plxna1*, *Plxna2*, *Plxna3*, *Plxnb1*, and *Plxnc1*. Similarly, the Ephrin receptors *Epha5*, *Epha8*, *Epha10*, *Ephb3*, and *Ephb6* are enriched in C-neurons. When we compared expression levels of receptors involved in signaling by the axon attractants Netrin-1 and Shh (Fig. 3f), we observed significant enrichment of *Dcc* and *Ptch2*. The UNC family members *Unc5a* and *Unc5d* are also preferentially expressed in C-neurons. Lastly, among neuronal cell adhesion molecules, we observed preferential expression of *Cntn2* (which encodes TAG-1), *Dscam*, *L1cam*, *Ncam1*, *Ncam2*, and *Nrcam* in C-neurons (Fig. 3g). Thus, consistent with their unique projection pattern, the axon guidance machinery in C-neurons is distinct from other neurons in the spinal cord.

We selected a small subset of candidate mRNAs that are strongly enriched and highly expressed in C-neurons for further analysis by *in situ* hybridization. Among these were *Chl1*, *Thsd7a*, *Dner*, and *Rgmb* (Fig. 3h), which encode membrane-bound cell surface proteins and could therefore be involved in C-axon guidance. *Chl1* encodes a member of the L1 family of adhesion molecules that is involved in neurite outgrowth (Hillenbrand, 1999; Montag-Sallaz, Schachner, & Montag, 2002), and *Thsd7a* encodes a thrombospondin repeat-rich protein involved in angiogenesis (Wang et al., 2011). The protein encoded by *Dner* (Delta/Notch-like EGF-related receptor) has been implicated in neuronal proliferation, differentiation, and neuritogenesis (Du, Wang, Zhang, Zhang, & Jiang, 2018; Eiraku, Hirata, Takeshima, Hirano, & Kengaku, 2002; Hsieh et al., 2013), and *Rgmb* encodes a glycosylphosphatidylinositol-anchored repulsive guidance molecule family member which regulates cell differentiation and nervous system patterning (Kam et al., 2016; Samad et al., 2005). *Sst*, *Kif26b*, *Mab21l2*, and *Lamp5* mRNAs are also highly enriched and expressed in C-neurons (Fig. 3h). *Sst* encodes the hormone Somatostatin (Patel, 1999); *Kif26b* encodes a kinesin that regulates cell polarity (Guillabert-Gourgues, 2016; Marikawa, Fujita, & Alarcon, 2004); *Mab21l2* encodes a nuclear protein that interacts with the BMP4 signaling

pathway and has been implicated in neural tube formation and eye morphogenesis (Baldessari, Badaloni, Longhi, Zappavigna, & Consalez, 2004; Z. X. Huang, 2016); *Lamp5* encodes a lysosome-associated membrane protein implicated in GABAergic neurotransmission (Tiveron et al., 2016). *In situ* hybridization for these mRNAs in brachial spinal cord transverse sections from E11.5 $Robo3^{Cre/+}$; $ROSA26^{LSL\text{-}tdTomato/+}$ embryos confirmed expression in various subgroups of C-neurons and revealed additional sites of expression (Fig 4a–h). Specifically, *Thsd7a* and *Rgmb* are expressed in dorsal spinal cord C-neurons and in the dorsal root ganglia (DRGs) (Fig. 4b and d), *Chl1* and *Kif26b* expression localizes to C-neurons in the intermediate spinal cord (Fig. 4a and f), and *Chl1* is also expressed in the FP (Fig. 4a). *Sst* is expressed in ventral spinal cord C-neurons as well as in the DRG and the ventral horn (Fig. 4e). *Dner* and *Mab21l2* expression co-localize with tdTomato signal along most or all of the dorso-ventral axis (Fig. 4c and g), and *Dner* is also expressed in the intermediate ventricular zone. *Lamp5* expression localizes to C-neurons in all but the most dorsally located C-neurons and is also detected in the ventral horn (Fig. 4h). Overall, these results are consistent with enrichment of the selected transcripts in C-neurons, as observed by RNA-Seq. Moreover, the preferential expression of different mRNAs in subpopulations of C-neurons indicates that these neurons are markedly diverse in their molecular profile.

3.3 Commissural neurons are generated from most progenitor populations during early and late neurogenesis.

To further explore the heterogeneity of C-neurons and elucidate their origins in the developing neural tube, we tracked them throughout spinal cord neurogenesis. First, we examined C-neuron cell body position in transverse sections of $Robo3^{Cre/+}$;$ROSA26^{LSL\text{-}tdTomato/+}$ brachial spinal cord at E10.5, E11.5, E12.5, and E14.5. We found that, at E10.5, the first C-neurons appear in the mediolateral portion of the neural tube, and that, between E11.5 and E14.5, they progressively populate all regions of the spinal cord except the ventral horn (Fig. 6a,b). This broad dispersal of C-neurons supports the idea that they arise from multiple progenitor populations spread along most of the dorsoventral neural tube axis.

Different progenitor domains in the embryonic spinal cord generate distinct subsets of postmitotic neurons that are defined by a combinatorial code of transcription factor expression (Alaynick et al., 2011; Lai et al., 2016). To begin to identify progenitor domains that give rise to C-neurons, we analyzed our E11.5 RNA-Seq data for the relative abundance of mRNAs that encode transcription factors specific to one or more subtypes of neurons (Fig. 6c, Table S1). *Barhl2* (expressed in postmitotic dI1 neurons), *Lhx1* and *Lhx5* (dI2, dI4/dIL_A, dI6, V0, and V1), *Tlx3* (dI3 and dI5), *Pax2* (dI4/dIL_A, dI6, $V0_D$, $V0_{CG}$, and V1), and *Sim1* (V3) are preferentially expressed in C-neurons. Conversely, *Isl1* and *Isl2* (dI3 and MNs) and *Foxp1* ($V1_{other}$ and lateral motor column MNs) are underrepresented in C-neurons. *Lhx2* (dI1) and *Bhlhe22* (also called *Bhlhb5*; dI6, V1, and V2) are expressed at comparable levels in C-neurons and non-commissural cells. Together, these data suggest that the entire population of E11.5 C-neurons encompasses substantial fractions of dI1, dI2, dI4/dIL_A, dI5/dIL_B, dI6, V0, and V3 neurons and few, if any, dI3 and MNs.

To directly examine the identity of C-neurons over time, we analyzed the expression of neuronal subtype-specific transcription factors by IHC in brachial spinal cord sections (see Materials and Methods and Table 2). We first sought to elucidate the origins of the earliest-born C-neurons that send pioneer axons across the spinal cord midline at E9.75. We found that the first few neurons immunoreactive for Robo3 express either Brn3a alone, Evx1/2 alone, Evx1/2 and Pax2 together, or Pax2 alone (Fig. 5a,b). Thus, the first C-neurons belong to the dI5 and $V0_V$ populations, either one or both of the $V0_C$ and $V0_G$ populations, and either one or more of the dI4, dI6, and $V0_D$ populations. Consistent with their origin from the pd4-p0 domains, pioneer C- neurons are located in the intermediate (with respect to the dorso-ventral axis) neural tube (Fig. 5a,b). Because many of these pioneer neurons are positive for the inhibitory neuron marker Pax2, we performed IHC for GAD67 at early E10.5 and found that a subset of mediolaterally located Robo3-positive neurons express this GABA biosynthetic enzyme (Fig. 5c). This result supports the idea that some of the pioneer C-neurons are GABAergic.

Next, we quantified the contribution of C-neurons to different progenitor domain-specific neuronal subtypes in E10.5, E11.5, E12.5, and E14.5 *Robo3*$^{Cre/+}$; *ROSA26*$^{LSL\text{-}tdTomato/+}$ mice. The dI1 subtype expresses Barhl2 and Lhx2 (Wilson, Shafer, Lee, & Dodd, 2008) and is comprised of ipsi- and contralaterally projecting neurons ($dI1_i$ and $dI1_c$, respectively); Lhx2 is downregulated in $dI1_i$ neurons by E12.5 (Wilson et al., 2008). Immunolabeling for Barhl2 and Lhx2 (Fig. 6d) revealed that, between E10.5 and E14.5, the fraction of Barhl2-positive neurons that are commissural (i.e. tdT^+) progressively increased with age (E10.5, 9.8±1.82%; E11.5, 37.6±3.13%; E12.5, 82.7±2.27%; E14.5, 94.7±2.31%) (Fig. 7a), suggesting that although Barhl2 is initially expressed in all dI1 neurons, its expression is maintained almost exclusively in the $dI1_c$ population. The fraction of $Lhx2^+$ neurons labeled by tdTomato also increases over time (E10.5, 6.0±3.08%; E11.5, 35.0±5.62%; E12.5, 83.2±3.05%; E14.5, 94.3±2.84%) (Fig. 7b), consistent with the notion that Lhx2 becomes an exclusive marker for $dI1_c$ neurons. We found that the small number of $Lhx2^+$ cells that remain tdT^- after E12.5 are exclusively localized to the most dorsomedial region of the spinal cord, suggesting that they are recently generated, later-born dI1 neurons that have not yet begun to express Robo3.

DI2 neurons express Lhx1/5 and are negative for Pax2, and a subset of dI2 neurons expresses Foxp1 at later developmental stages (E12.5 and E14.5) (Francius et al., 2013; Wong, 2009). We used IHC for these markers to identify dI2 neurons (Fig. 6e,h). Consistent with the idea that the majority of dI2 neurons project axons contralaterally (Avraham et al., 2009), we found that, at E10.5 and E11.5, 54.8±20.09% and 73.4±0.54%, respectively, of all dI2 neurons are commissural (Fig. 7c); at E12.5 and E14.5, 79.5±5.30% and 89.9±3.11% of $Foxp1^+$ dI2 neurons, respectively, are commissural (Fig. 7c).

DI3 neurons express Tlx3 and Islet1/2. Immunolabeling for these transcription factors (Fig. 6f) revealed that dI3 neurons do not contribute to the C-neuron population, and vice versa.

DI4 neurons and the later-born dIL_A neurons express Lhx1/5 and Pax2. Lhx1/5 and Pax2 immunolabeling at E10.5 and E11.5 (Fig. 6e) showed that 21.3±5.50% and 37.6±8.96% of dI4/dIL_A neurons are commissural, respectively (Fig. 7d). Pax2 immunolabeling alone at

E12.5 and E14.5 (Fig. 6g) showed that, 84.0±1.98% and 94.46±0.86% of the dI4/dIL$_A$ population are commissural, respectively (Fig. 7d). At E12.5 and E14.5, the only dI4/dIL$_A$ neurons that are tdT$^-$ are found near the ventricular zone (data not shown), and are likely recently born cells that have not begun to express detectable levels of tdTomato yet. Together these data support the idea that most, if not all, dI4/dIL$_A$ neurons are commissural.

Tlx3 is expressed in dI3, dI5, and dIL$_B$ neurons, while Islet1/2 expression is exclusive to dI3 and MNs. IHC for Tlx3 and Islet1/2 (Fig. 6f) showed that C-neurons comprised 17.4±3.81%, 33.9±7.18%, 6.6±0.60%, and 5.18±0.07% of the dI5/dIL$_B$ population at E10.5, E11.5, E12.5, and E14.5, respectively (Fig. 7e), indicating that the vast majority of dI5/dIL$_B$ neurons project ipsilaterally.

Neurons in the V0 domain express Lhx1/5, but not Bhlhb5 or Foxp1, at E10.5 and E11.5. Using the relevant antibody combinations (Fig. 6h), we found that 26.2±1.66% and 52.1±2.03% of V0 neurons at E10.5 and E11.5, respectively, are commissural (Fig. 7f).

DI6 and V1$_{Ren/IaIN}$ populations express Lhx1/5 and Bhlhb5, and though they are spatially segregated at E10.5, these neurons intermingle by E11.5. Immunolabeling for Lhx1/5 and Bhlhb5 (Fig. 6h) revealed that, at E10.5, 21.3±2.35% of dI6 neurons and 7.5±1.16% of V1$_{Ren/IaIN}$ neurons are commissural (Fig. 7g). At E11.5, E12.5, and E14.5, 21.1±3.12%, 29.4±2.80% and 44.4±3.54% of the combined dI6 and V1$_{Ren/IaIN}$ populations are commissural, respectively. We observed that most dI6 neurons at E10.5 appeared to be recently born and in the initial stages of migrating laterally from the ventricular zone. TdTomato was not detectable in these medially located dI6 neurons, whereas many of the dI6 neurons that had migrated further were expressing tdTomato.

The V1$_{other}$ neurons express Foxp1, Bhlhb5, and Lhx1/5. IHC for these markers (Fig. 6h) showed that 10.62±0.70%, 21.3±2.98%, 50.0±2.59%, and 59.8±4.19% of V1$_{other}$ neurons are commissural at E10.5, E11.5, E12.5, and E14.5, respectively (Fig. 7h).

V2 neurons express Bhlhb5, but not Lhx1/5 or Foxp1. Immunolabeling for the relevant transcription factors (Fig. 6h) revealed that none of the V2 neurons are commissural.

Together, our results demonstrate that C-neurons are represented in the dI1, dI2, dI4/dIL$_A$, dI5/dIL$_B$, dI6, V0, and V1 populations, while the dI3 and V2 populations do not contain C-neurons. We quantified the contribution of different spinal cord neuron subtypes to the entire C-neuron population at E10.5, E11.5, E12.5, and E14.5 (Fig. 7i, Table 3). We uncovered a substantial (≈20%) contribution of dI1 neurons to the C-neuron pool during early neurogenesis, as well as a major (≈50%) combined contribution of dI4/dIL$_A$. Further, our analysis identified a large variety of neuronal subtypes, including some that have been considered as exclusively ipsilaterally projecting (see Discussion), that comprise smaller subsets of the total C-neuron population.

3.4 *Robo3^{Cre}*-mediated fate mapping uncovers positional and molecular diversity of mature commissural neurons.

The spatial arrangement of neurons generated from different spinal cord progenitor domains is eroded by extensive migration and intermixing of neuronal subtypes over the course of

development. To uncover the final locations and mature molecular identities of C-neurons in the adult spinal cord, we mapped their fate in *Robo3*$^{Cre/+}$; *ROSA26*$^{LSL\text{-}tdTomato/+}$ mice. While Robo3 expression in the developing neural tube is transient (data not shown), tdTomato expression persists in the adult *Robo3*$^{Cre/+}$; *ROSA26*$^{LSL\text{-}tdTomato/+}$ spinal cord (Fig. 8a). Staining of brachial spinal cord transverse sections for the neuronal marker NeuN and nuclear Hoechst stain revealed that tdT^{+} cells are exclusively neuronal and comprise 53.6±1.68% of all neurons and 9.1±0.26% of all cells in adult spinal cord (Fig. 8a). To verify that tdTomato expression labels all mature C- neurons, we injected DiO unilaterally into the white matter near the ventral midline. Just as in the developing spinal cord (Fig. 2b), 100% of DiO^{+} cells contralateral to the injection site are tdT^{+} (Fig. 8b), confirming that all adult C-neurons continue to express tdTomato. DiO labeling efficiency in these experiments (n=3) is 36.4±7.03% of contralateral tdT^{+} cells and captures neurons distributed throughout the spinal cord.

To characterize the distribution of C-neurons throughout the gray matter of the spinal cord, we used IHC for markers that identify different dorsal horn laminae, namely NK-1R, IB4, PKC-γ, CGRP, Sst, GAD67, and CB (Fig. 9a, left column). C-neurons within different laminae (see Materials and Methods for definition) of adult *Robo3*$^{Cre/+}$; *ROSA26*$^{LSL\text{-}tdTomato/+}$ brachial spinal cord transverse sections were counted (Fig. 9a, middle and right columns). We found that lamina I contains 7.76±0.24% of C-neurons, outer lamina II 8.03±0.67%, inner lamina II 10.60±0.86%, and lamina III 8.35±4.42% of C-neurons, while 65.26±4.42% of all C-neurons are found in laminae IV-X (Fig. 9b, left panel). Visual inspection of C-neuron distribution indicates that a large fraction of C-neurons ventral to lamina III resides in laminae IV and V of the deep dorsal horn, some C- neurons can be found in lamina X surrounding the central canal, and very few are located in the ventral horn (Fig. 9b, right panel). Thus, C-neurons are found in regions that process somatosensory information of various modalities. To determine whether C-neurons might receive direct synaptic inputs from DRG neurons, we labeled spinal cord sections from *Robo3*$^{Cre/+}$; *ROSA26*$^{LSL\text{-}tdTomato/+}$ mice for markers of sensory axons. We frequently observed sensory axon terminals positive for members of the Trk family of neurotrophin receptors – specifically, TrkA, TrkB, and TrkC – in close apposition to dorsal horn C-neuron cell bodies (Fig. 10a–c), consistent with the idea that DRG axons make synaptic contacts with C-neurons. Similarly, axons positive for CGRP, a marker for peptidergic afferents (Todd, 2010), and NK-1R, which is expressed in a subset of small-diameter primary sensory neurons (Li, 1998), appear to make synaptic contact with C-neurons in the dorsal horn (Fig. 10d,e). Together, these data suggest that C-neurons help relay and/or process multiple somatosensory modalities, in some instances receiving direct input from DRG sensory neurons.

To begin to understand the molecular diversity of mature C-neurons, we labeled various neuronal subtypes with antibodies in brachial spinal cord transverse sections of *Robo3*$^{Cre/+}$;*ROSA26*$^{LSL\text{-}tdTomato/+}$ mice (Fig. 11a–g). PKC-γ is expressed in excitatory interneurons that receive inputs from low-threshold mechanoreceptors (Neumann, Braz, Skinner, Llewellyn-Smith, & Basbaum, 2008); NK-1R identifies ascending projection neurons located in dorsal horn lamina I (Todd, 2010); CGRP labels ventral horn MNs and other neurons in the superficial dorsal horn, lamina X, and ventral spinal cord (Eftekhari &

Edvinsson, 2011; Gibson et al., 1984; Kim, Sunagawa, Kobayashi, Shin, & Takayama, 2016); Tlx3 marks dI5 excitatory neurons in the dorsal horn (Xu et al., 2008); Pax2 identifies subsets of mature inhibitory neurons (Cheng et al., 2004; Larsson, 2017); staining for GABA identifies neurons that synthesize this inhibitory neurotransmitter; CB and CR are calcium-binding proteins expressed in subsets of almost exclusively excitatory neurons (Albuquerque, 1999; Antal, 1991; Ren & Ruda, 1994). We found that PKC-γ^+ neurons do not contribute to the commissural population (Fig. 11a), 2.14±0.31% of C-neurons belong to the NK-1R$^+$ population (Fig. 11b), 3.61±0.63% are positive for CGRP (Fig. 11c), 12.67±2.13% express Tlx3 (Fig. 11d), 51.78±9.27% are classified as Pax2$^+$ (Fig. 11e), 39.57±4.32% belong to the GABA$^+$ population (Fig. 11f), 5.66±0.56% are positive for CB but not CR, 12.62±3.78% do not express CB but are CR$^+$, and 2.91±0.89% are both CB$^+$ and CR$^+$ (Fig. 11g). Conversely, C-neurons comprise 23.9±2.75% of the NK-1R$^+$ population, 90.87±2.61% of the CGRP$^+$ population, 16.32±1.83% of the Tlx3$^+$ population, 35.60±6.97% of the Pax2$^+$ population, 30.86±4.71% of the GABA$^+$ population, 18.7±1.74% of the CB$^+$/CR$^-$ population, 35.22±0.63% of the CB$^-$/CR$^+$ population, and 29.43±5.04% the CB$^+$/CR$^+$ population (Fig. 11h). Thus, mature C-neurons exhibit broad molecular heterogeneity, supporting the idea that they fulfill a variety of functions within different spinal cord circuits. Consistent with this notion, immunostaining for the vGluT family members and two markers of inhibitory axons – neuropeptide Y (NPY), which identifies a subset of GABAergic inputs (Todd, 2010), and the neuronal glycine transporter GlyT2 – labeled axon terminals that appear to make contact with C-neurons (Fig. 10f–j). These results support the idea that mature C-neurons are not only heterogeneous in terms of their molecular makeup, but also their presynaptic inputs.

4. DISCUSSION

C-neurons project axons across the spinal cord midline to connect the two halves of the nervous system. The developmental origin and differentiation program of C-neurons, as well as their final position, molecular makeup, connectivity, and function in different spinal cord circuits, varies widely. While this heterogeneity has long been appreciated, lack of genetic access to the entire C-neuron population has impeded the systematic exploration of its diversity and limited insights gained from previous studies of C-neuron development and function. To overcome this constraint, we generated *Robo3*^{Cre} mice, which express Cre recombinase specifically in C-neurons and allow their labeling and manipulation during both development and adulthood. We used *Robo3*^{Cre} mice to characterize the various origins and bulk gene expression profile of C-neurons during development. Our analysis identifies transcripts that are enriched in C-neurons and reveals new details about the considerable heterogeneity in C-neuron developmental lineage and molecular profile. Further, we used *Robo3*^{Cre} mice to track C-neurons into adulthood and stratify this neuronal population in the mature spinal cord. We uncover an extensive positional and molecular heterogeneity and provide evidence for participation of C-neurons in diverse spinal cord circuits.

4.1 The *Robo3*^{Cre} mouse line as a genetic tool to access spinal commissural neurons

We generated a *Robo3*^{Cre} allele that drives Cre DNA recombinase expression from the endogenous *Robo3* locus, and we validated the C-neuron specificity of this new mouse line

by multiple means. First, crossing of *Robo3*^{Cre} mice to a Cre-dependent fluorescent reporter and analysis via Robo3 IHC demonstrated that Cre activity faithfully recapitulates Robo3 expression in the spinal cord, with minimal temporal delay. Second, this was further corroborated by using the *Robo3*^{Cre} line to delete a conditional *Robo3* allele, which results in complete loss of Robo3 expression and absence of the spinal cord ventral commissure. Third, we combined retrograde tracing with labeling via a Cre-dependent reporter to show that *Robo3*^{Cre}-mediated recombination captures all C-neurons, both during development and in the adult spinal cord, as all contralaterally traced neurons are positive for reporter expression. These experiments also indicate that Cre activity is exclusive to C-neurons, as retrograde tracing from the lateral funiculus, where axons from many ipsilaterally projecting neurons enter the fiber tracts, only labels reporter-negative cells ipsilateral to the dye injection site. However, since labeling efficiency in these retrograde tracing experiments is always below 100%, we cannot completely exclude the possibility that a small subset of ipsilaterally projecting neurons exhibit *Robo3*^{Cre}-mediated recombination. Importantly, C-axon projections in mice carrying one *Robo3*^{Cre} allele appear grossly normal, consistent with previous reports that loss of one Robo3 allele does not affect C-axon guidance to the midline (Jaworski et al., 2015; Sabatier, 2004). Together, these results show that *Robo3* is expressed in all C-neurons and no other cells within the spinal cord and strongly support the notion that the *Robo3*^{Cre} line provides selective and complete access to spinal C-neurons without disrupting their wiring.

The *Robo3*^{Cre} mouse overcomes the limitations of prior approaches to label and target C-neurons and their projections, which have relied on IHC markers, tracing, or other reporter and Cre lines. While antibodies against Robo3 and TAG-1 stain precrossing C-axons, they do not allow visualization of postcrossing axons and label cell bodies poorly or not at all; moreover, expression of Robo3 and TAG-1 are restricted to a narrow developmental time window. Antero- or retrograde axonal tracing via dye injection is limited to cohorts of C-neurons and also captures ipsilaterally projecting neurons close to the injection site. Lastly, expression of reporter genes or DNA recombinases in other mouse lines does not provide the same specificity as the *Robo3*^{Cre} line; e.g. *Math1::lacZ* and *Math1::Cre* transgenic mice have been used to label and manipulate C-neurons, but these lines drive expression in the entire dI1 population and are therefore neither specific for C-neurons nor do they capture non-dI1 C-neurons (Helms & Johnson, 1998; Yamauchi, Phan, & Butler, 2008). *Robo3*^{Cre} mice, on the other hand, allow specific, complete, and permanent labeling of C-neurons in combination with Cre-dependent reporter lines. They may also be used for other applications, such as C-neuron-specific deletion of genes, expression of genetic components for viral tracing or translational profiling experiments, and intersectional genetic targeting of C-neuron subpopulations.

4.2 The commissural neuron transcriptome

Various receptors involved in C-axon guidance have been previously identified. Some of these, e.g. Robo1 and Robo2, are broadly expressed in the spinal cord. Others, including Nrp2 and DCC appear enriched in, but not exclusive to, C-neurons. Additional C-neuron-enriched molecules are likely involved in neuronal differentiation and axon guidance, but a systematic evaluation of C- neuron gene expression was previously not feasible, as this

neuronal population could not be isolated in its entirety. We sorted E11.5 C-neurons based on a *Robo3*^{Cre}-activated fluorescent reporter and used RNA-Seq to generate a bulk gene expression profile that was compared to non-fluorescent spinal cord cells, which include diverse classes of neuronal, progenitor, and endothelial cells. Our results confirm C-neuron enrichment of transcripts that encode receptors for Netrins, Slits, Semaphorins, Ephrins, and Shh, as well as numerous immunoglobulin superfamily cell adhesion molecules. Our analysis also reveals a large number of additional highly expressed and significantly enriched mRNAs in C-neurons, providing a list of novel candidate genes for future functional studies of C-neuron development. We validated C-neuron-specific expression of a few select transcripts by ISH. The preferential expression patterns of these mRNAs in distinct C-neuron populations supports the RNA-Seq data and highlights the molecular heterogeneity of developing C-neurons. It is possible that some molecules enriched in C-neurons were not captured in our results due to the high stringency of FAC-sorting tdT^{+} cells, transcript enrichment in very small subsets of C-neurons, or limiting our analysis to mRNAs (not proteins).

4.3 Diversity of commissural neuron developmental origin

Multiple progenitor domains in the developing spinal cord give rise to C-neurons. However, a comprehensive, quantitative analysis of C-neuron developmental origin has not been conducted, likely because C-neuron-specific IHC markers are not expressed throughout the entire time window of neurogenesis. We combined *Robo3*^{Cre}-dependent genetic labeling with IHC detection of markers for the postmitotic offspring of different progenitor classes to generate a developmental fate map of C-neurons. Consistent with prior reports, we found that subsets of dI1, dI2, dI5/dIL$_B$, dI6, and V0 neurons are commissural. We also show that dI3, V2, and, as expected, MNs do not contribute to the C-neuron population. Interestingly, most dI4/dIL$_A$ neurons are commissural and account for more than half of all C-neurons, which has not been appreciated previously. A substantial portion of V1 neurons, including both the V1$_{Ren/IaIN}$ and V1$_{other}$ subcategories, are also commissural, which has not been described before (Goulding & Pfaff, 2005; Kiehn, 2011), and our findings further underscore the heterogeneity of V1 neurons (Bikoff et al., 2016). We also provide evidence that the earliest-born C-neurons that send axons towards the FP originate from the pd4-p0 domains midway along the dorsoventral axis, suggesting that the axons originating from these C-neuron subtypes pioneer the trajectory towards and across the midline. At least some of these pioneer neurons appear to be GABAergic, consistent with previous reports that describe expression of GABA biosynthetic enzymes in C-neurons located in the early, intermediate mouse and rat spinal cord (Kosaka, Kin, Tatetsu, Uema, & Takayama, 2012; Phelps, Alijani, & Tran, 1999).

The use of IHC markers to identify neuronal classes has several limitations. First, expression of transcription factors that are thought to mark defined types of postmitotic neurons can dynamically change over time, even within subgroups of these populations. In one particularly complex example, early dI1 neurons express Barhl2 and Lhx2, but dI1$_i$ neurons appear to subsequently downregulate Barhl2 (this study) and Lhx2 (Ding, Joshi, Xie, Xiang, & Gan, 2012; Wilson et al., 2008) earlier than the dI1$_c$ subset. At later stages of embryonic development, the majority of dI1 neurons that maintain Barhl2 and/or Lhx2 expression is

therefore commissural, and there is a substantial fraction of ipsilaterally projecting dI1 neurons that is not captured by these markers. Further complicating the picture, Barhl2 and Lhx2 do not continuously label all $dI1_c$ neurons, making these transcription factors imperfect markers even for just this subclass (Ding et al., 2012; Wilson et al., 2008). Moreover, antibody labeling for subtype markers can produce results that seem to contradict studies using genetic reporters. Our results indicate that the majority of Barhl2-positive neurons are commissural, while a *Barhl2*^{lacZ} reporter allele appears to label at least as many $dI1_i$ as $dI1_c$ neurons (Ding et al., 2012). Posttranscriptional regulation that leads to preferential Barhl2 protein accumulation in $dI1_c$ neurons may well explain this discrepancy. Second, using IHC for the relevant transcription factor combinations, the early-born dI4 and dI5 classes are indistinguishable from the later-born dIL_A and dIL_B neurons, respectively. Nonetheless, the marked increase in the contribution of dI4/dIL_A neurons to the C-neuron population at E12.5 and a complementary increase in the fraction of dI4/dIL_A neurons that are commissural suggests that the overwhelming majority of dIL_A neurons that comprise the second wave of neurogenesis is commissural. Conversely, the fraction of dI5/dIL_B neurons that are commissural prominently decreases at E12.5 and E14.5, as does the contribution of dI5/dIL_B neurons to the C-neuron population at these ages, indicating that most or all of the C-neurons determined to be dI5/dIL_B were born exclusively during the first wave of neurogenesis (i.e, they are dI5 neurons). Third, our lack of access to reliable IHC markers for V3 neurons, as well as V0 at E12.5 and E14.5, prevented us from analyzing these classes in isolation. However, prior studies have shown that V3 neurons make connections mostly, if not exclusively, in the contralateral spinal cord (Zhang et al., 2008). Consistent with this idea, our RNA-Seq data demonstrate that the V3 marker *Sim1* is preferentially expressed in C-neurons. Despite these caveats, our analysis provides a detailed stratification of C-neurons with respect to their origins from different progenitor classes and underscores the extensive developmental diversity of these neurons. These results can serve as a framework for future studies aimed at identifying the molecular programs that (1) unify all C-neuron subtypes and ensure axon crossing of the midline and (2) ultimately translate the different developmental identities into the various connectivity patterns and functions of mature C-neurons.

4.4 Heterogeneity of adult commissural neurons

Previous studies have yielded some information on the position, neurotransmitter phenotype, and circuit function of C-neurons in the adult spinal cord. Most of these analyses relied on axonal tracing, electrophysiology, or spinal cord lesions, none of which capture the entire C-neuron population and/or suffer from lack of cellular resolution. We used *Robo3*^{Cre} mice to permanently label C-neurons beyond embryogenesis and characterized the location, molecular identity, and presynaptic inputs of C-neurons in the adult. Consistent with their extensive diversity during development, C-neurons exhibit a broad distribution throughout the mature spinal cord and considerable molecular heterogeneity. Their presence in nearly all spinal cord laminae suggests that they participate in a variety of circuit functions. The high concentration of C-neurons in the dorsal horn, along with the observed close apposition of DRG afferent nerve terminals support the idea that C-neurons help relay, process, and/or integrate nociceptive, thermoreceptive, pruriceptive, mechanoreceptive, and proprioceptive somatosensory information. The more ventrally located C-neurons likely control left-right coordination of motor output through the CPG, as previously reported (Goulding & Pfaff,

2005; Kiehn, 2011). Additional experiments, leveraging the genetic access provided by the *Robo3*^{Cre} line for transsynaptic tracing, electrophysiology, and optogenetic analyses, will be required to elucidate the input-output relationships and circuit functions of C-neurons.

Further C-neuron heterogeneity is highlighted by our analysis of markers for classes of adult neurons, revealing various excitatory subtypes and GABAergic neurons in the C-neuron population. Inputs to C-neurons include peptidergic, inhibitory, and glutamatergic nerve terminals, increasing diversity of this neuronal population further. Future studies are needed to fully explore the heterogeneity of mature C-neurons and correlate different molecular parameters with functions. Exploiting the entry point provided through the *Robo3*^{Cre} line for deep molecular profiling, e.g. via single-cell RNA-Seq, will be a powerful approach to tackle this problem.

Supplementary Material

Refer to Web version on PubMed Central for supplementary material.

ACKNOWLEDGEMENTS

We thank the Gene Targeting, Flow Cytometry, and Genomics Centers at The Rockefeller University for help with generating the *Robo3*^{Cre} mouse line and carrying out cell sorting and RNA- Seq experiments. We also thank Yonghong Zhou and Julia Schoenewald for technical assistance, David Sheinberg, Scott Susi, and Seth Akers-Campbell for help with generating cell body distribution plots, and the members of the Jaworski laboratory for thoughtful comments on the manuscript. We are grateful to Sarah Ross (University of Pittsburgh, Pittsburgh PA), Christopher Wright (Vanderbilt University, Nashville, TN), and Carmen Birchmeier (Max-Delbrück-Centrum for Molecular Medicine, Berlin, Germany) for generously providing antibodies.

This work was supported by the National Institutes of Health [R01 NS095908 to A.J., T32 NS062443 and T32 MH020068 to A.J.T., R25 NS080686 to B.V.C.], the Brain Research Foundation [BRFSG-2016–11 to A.J.], the Agency for Science, Technology and Research of Singapore [to S.T.], The Rockefeller University, and Brown University.

REFERENCES

Airaksinen MS, Eilers J, Garaschuk O, Thoenen H, Konnerth A, & Meyer M (1997). Ataxia and altered dendritic calcium signaling in mice carrying a targeted null mutation of the calbindin D28k gene. Proc Natl Acad Sci U S A, 94(4), 1488–1493. [PubMed: 9037080]

Alaynick WA, Jessell TM, & Pfaff SL (2011). SnapShot: Spinal Cord Development. Cell, 146(1), 178–178.e171. doi:10.1016/j.cell.2011.06.038 [PubMed: 21729788]

Albuquerque CL CJ; Jackson AC; MacDermott AB. (1999). Subpopulations of GABAergic and non-GABAergic rat dorsal horn neurons express Ca2+-permeable AMPA receptors. European Journal of Neuroscience, 11, 2758–2766. [PubMed: 10457172]

Antal MP,E; Chalmers J; Minson JB; Llewellyn-Smith I; Heizmann CW, Somogyi P. (1991). Different populations of parvalbumin- and calbindin-D28k-immunoreactive neurons contain GABA and accumulate 3H-D-aspartate in the dorsal horn. The Journal of Comparative Neurology, 314, 114–124. [PubMed: 1797867]

Averill S, McMahon SB, Clary DO, Reichardt LF, & Priestley JV (1995). Immunocytochemical localization of trkA receptors in chemically identified subgroups of adult rat sensory neurons. Eur J Neurosci, 7(7), 1484–1494. [PubMed: 7551174]

Avraham O, Hadas Y, Vald L, Zisman S, Schejter A, Visel A, & Klar A (2009). Transcriptional control of axonal guidance and sorting in dorsal interneurons by the Lim-HD proteins Lhx9 and Lhx1. Neural Dev, 4, 21. doi:10.1186/1749-8104-4-21 [PubMed: 19545367]

Baldessari D, Badaloni A, Longhi R, Zappavigna V, & Consalez GG (2004). MAB21L2, a vertebrate member of the Male-abnormal 21 family, modulates BMP signaling and interacts with SMAD1. BMC Cell Biol, 5(1), 48. doi:10.1186/1471-2121-5-48 [PubMed: 15613244]

Bikoff JB, Gabitto MI, Rivard AF, Drobac E, Machado TA, Miri A, … Jessell TM (2016). Spinal Inhibitory Interneuron Diversity Delineates Variant Motor Microcircuits. Cell, 165(1), 207–219. doi:10.1016/j.cell.2016.01.027 [PubMed: 26949184]

Borowska J, Jones CT, Zhang H, Blacklaws J, Goulding M, & Zhang Y (2013). Functional subpopulations of V3 interneurons in the mature mouse spinal cord. J Neurosci, 33(47), 18553–18565. doi:10.1523/JNEUROSCI.2005-13.2013 [PubMed: 24259577]

Charron FS,E; Jeong J; McMahon AP; Tessier-Lavigne M. (2003). The Morphogen Sonic Hedgehog Is an Axonal Chemoattractant that Collaborates with Netrin-1 in Midline Axon Guidance. Cell, 113, 11–23. [PubMed: 12679031]

Chedotal A (2014). Development and plasticity of commissural circuits: from locomotion to brain repair. Trends Neurosci, 37(10), 551–562. doi:10.1016/j.tins.2014.08.009 [PubMed: 25220044]

Chen Z, Gore BB, Long H, Ma L, & Tessier-Lavigne M (2008). Alternative splicing of the Robo3 axon guidance receptor governs the midline switch from attraction to repulsion. Neuron, 58(3), 325–332. doi:10.1016/j.neuron.2008.02.016 [PubMed: 18466743]

Cheng L, Arata A, Mizuguchi R, Qian Y, Karunaratne A, Gray PA, … Ma Q (2004). Tlx3 and Tlx1 are post-mitotic selector genes determining glutamatergic over GABAergic cell fates. Nat Neurosci, 7(5), 510–517. doi:10.1038/nn1221 [PubMed: 15064766]

Corleto JA, Bravo-Hernandez M, Kamizato K, Kakinohana O, Santucci C, Navarro MR, … Marsala M (2015). Thoracic 9 Spinal Transection-Induced Model of Muscle Spasticity in the Rat: A Systematic Electrophysiological and Histopathological Characterization. PLoS One, 10(12), e0144642. doi:10.1371/journal.pone.0144642 [PubMed: 26713446]

Dickson BJ, & Zou Y (2010). Navigating intermediate targets: the nervous system midline. Cold Spring Harb Perspect Biol, 2(8), a002055. doi:10.1101/cshperspect.a002055 [PubMed: 20534708]

Ding Q, Joshi PS, Xie ZH, Xiang M, & Gan L (2012). BARHL2 transcription factor regulates the ipsilateral/contralateral subtype divergence in postmitotic dI1 neurons of the developing spinal cord. Proc Natl Acad Sci U S A, 109(5), 1566–1571. doi:10.1073/pnas.1112392109 [PubMed: 22307612]

Dodd J, Morton SB, Karagogeos D, Yamamoto M, & Jessell TM (1988). Spatial regulation of axonal glycoprotein expression on subsets of embryonic spinal neurons. Neuron, 1(2), 105–116. [PubMed: 3272160]

Dressler GR, & Douglass EC (1992). Pax-2 is a DNA-binding protein expressed in embryonic kidney and Wilms tumor. Proc Natl Acad Sci U S A, 89(4), 1179–1183. [PubMed: 1311084]

Du J, Wang X, Zhang X, Zhang X, & Jiang H (2018). DNER modulates the length, polarity and synaptogenesis of spiral ganglion neurons via the Notch signaling pathway. Mol Med Rep, 17(2), 2357–2365. doi:10.3892/mmr.2017.8115 [PubMed: 29207144]

Eftekhari S, & Edvinsson L (2011). Calcitonin gene-related peptide (CGRP) and its receptor components in human and rat spinal trigeminal nucleus and spinal cord at C1-level. BMC Neurosci, 12, 112. [PubMed: 22074408]

Eide AL, Glover JC, Kjaerulff O, & Kiehn O (1999). Characterization of commissural interneurons in the lumbar region of the neonatal rat spinal cord. The Journal of Comparative Neurology, 403, 332–345. [PubMed: 9886034]

Eiraku M, Hirata Y, Takeshima H, Hirano T, & Kengaku M (2002). Delta/notch-like epidermal growth factor (EGF)-related receptor, a novel EGF-like repeat-containing protein targeted to dendrites of developing and adult central nervous system neurons. J Biol Chem, 277(28), 25400–25407. doi:10.1074/jbc.M110793200 [PubMed: 11950833]

Erlander MG, Tillakaratne NJ, Feldblum S, Patel N, & Tobin AJ (1991). Two genes encode distinct glutamate decarboxylases. Neuron, 7(1), 91–100. [PubMed: 2069816]

Fasano C, Rocchetti J, Pietrajtis K, Zander JF, Manseau F, Sakae DY, … El Mestikawy S (2017). Regulation of the Hippocampal Network by VGLUT3-Positive CCK- GABAergic Basket Cells. Front Cell Neurosci, 11, 140. doi:10.3389/fncel.2017.00140 [PubMed: 28559797]

Francius C, Harris A, Rucchin V, Hendricks TJ, Stam FJ, Barber M, … Clotman F (2013). Identification of multiple subsets of ventral interneurons and differential distribution along the rostrocaudal axis of the developing spinal cord. PLoS One, 8(8), e70325. doi:10.1371/journal.pone.0070325 [PubMed: 23967072]

Genc B, Ozdinler PH, Mendoza AE, & Erzurumlu RS (2004). A chemoattractant role for NT-3 in proprioceptive axon guidance. PLoS Biol, 2(12), e403. doi:10.1371/journal.pbio.0020403 [PubMed: 15550985]

Gibson SJ, Polak JM, Bloom SR, Sabate IM, Mulderry PM, Ghatei MA, … Rosenfeld MG (1984). Calcitonin gene-related peptide immunoreactivity in the spinal cord of man and of eight other species. J Neurosci, 4(12), 3101–3111. [PubMed: 6209366]

Goulding M (2009). Circuits controlling vertebrate locomotion: moving in a new direction. Nat Rev Neurosci, 10(7), 507–518. doi:10.1038/nrn2608 [PubMed: 19543221]

Goulding M, & Pfaff SL (2005). Development of circuits that generate simple rhythmic behaviors in vertebrates. Curr Opin Neurobiol, 15(1), 14–20. doi:10.1016/j.conb.2005.01.017 [PubMed: 15721739]

Gouti M, Metzis V, & Briscoe J (2015). The route to spinal cord cell types: a tale of signals and switches. Trends Genet, 31(6), 282–289. doi:10.1016/j.tig.2015.03.001 [PubMed: 25823696]

Guillabert-Gourgues AJ-V,B; Bats ML; Sewduth RN; Franzi N; Peghaire C; Jeanningros S; Moreau C; Roux E; Larrieu-Lahargue F; Dufourcq P; Couffinhal T; Duplaa C. (2016). Kif26b controls endothelial cell polarity through the Dishevelled/Daam1-dependent planar cell polarity–signaling pathway. Mol Biol Cell, 27(6), 941–953. doi:10.1091/mbc.E14-08-1332) [PubMed: 26792835]

Harmann PA, Chung K, Briner RP, Westlund KN, & Carlton SM (1988). Calcitonin gene-related peptide (CGRP) in the human spinal cord: a light and electron microscopic analysis. J Comp Neurol, 269(3), 371–380. doi:10.1002/cne.902690305 [PubMed: 3259588]

Helms AW, & Johnson JE (1998). Progenitors of dorsal commissural interneurons are defined by MATH1 expression. Development, 125(5), 919–928. [PubMed: 9449674]

Helms AW, & Johnson JE (2003). Specification of dorsal spinal cord interneurons. Current Opinion in Neurobiology, 13(1), 42–49. doi:10.1016/s0959-4388(03)00010-2 [PubMed: 12593981]

Heusner CL, Beutler LR, Houser CR, & Palmiter RD (2008). Deletion of GAD67 in dopamine receptor-1 expressing cells causes specific motor deficits. Genesis, 46(7), 357–367. doi:10.1002/dvg.20405 [PubMed: 18615733]

Hillenbrand RMM; Montag D; Schachner M. (1999). The close homologue of the neural adhesion molecule L1 (CHL1): patterns of expression and promotion of neurite outgrowth by heterophilic interactions. European Journal of Neuroscience, 11, 813–826. [PubMed: 10103075]

Hsieh FY, Ma TL, Shih HY, Lin SJ, Huang CW, Wang HY, & Cheng YC (2013). Dner inhibits neural progenitor proliferation and induces neuronal and glial differentiation in zebrafish. Dev Biol, 375(1), 1–12. doi:10.1016/j.ydbio.2013.01.007 [PubMed: 23328254]

Huang HY, Cheng JK, Shih YH, Chen PH, Wang CL, & Tsaur ML (2005). Expression of A-type K channel alpha subunits Kv 4.2 and Kv 4.3 in rat spinal lamina II excitatory interneurons and colocalization with pain-modulating molecules. Eur J Neurosci, 22(5), 1149–1157. doi:10.1111/j.1460-9568.2005.04283.x [PubMed: 16176357]

Huang ZX (2016). The Male Abnormal Gene Family 21 (Mab21) Members Regulate Eye Development. Current molecular medicine, 16(7), 660–EOA. [PubMed: 27558071]

Jaworski A, Tom I, Tong RK, Gildea HK, Koch AW, Gonzalez LC, & Tessier-Lavigne M (2015). Operational redundancy in axon guidance through the multifunctional receptor Robo3 and its ligand NELL2. Science, 350(6263), 961–965. [PubMed: 26586761]

Jessell TM (2000). Neuronal specification in the spinal cord- inductive signals and transcriptional codes. Nature Reviews, 1, 20–29.

Junge HJ, Yung AR, Goodrich LV, & Chen Z (2016). Netrin1/DCC signaling promotes neuronal migration in the dorsal spinal cord. Neural Dev, 11(1), 19. doi:10.1186/s13064-016-0074-x [PubMed: 27784329]

Kadison SR, Makinen T, Klein R, Henkemeyer M, & Kaprielian Z (2006). EphB receptors and ephrin-B3 regulate axon guidance at the ventral midline of the embryonic mouse spinal cord. J Neurosci, 26(35), 8909–8914. doi:10.1523/JNEUROSCI.1569-06.2006 [PubMed: 16943546]

Kam JW, Dumontier E, Baim C, Brignall AC, Mendes da Silva D, Cowan M, … Cloutier JF (2016). RGMB and neogenin control cell differentiation in the developing olfactory epithelium. Development, 143(9), 1534–1546. doi:10.1242/dev.118638 [PubMed: 27143755]

Kaneyama T, & Shirasaki R (2018). Post-crossing segment of dI1 commissural axons forms collateral branches to motor neurons in the developing spinal cord. J Comp Neurol, 526(12), 1943–1961. doi:10.1002/cne.24464 [PubMed: 29752714]

Kennedy TES,T; de la Torre JR; Tessier-Lavigne M. (1994). Netrins are diffusible chemotropic factors for commissural axons in the embryonic spinal cord. Cell, 78, 425–435. [PubMed: 8062385]

Kiehn O (2011). Development and functional organization of spinal locomotor circuits. Curr Opin Neurobiol, 21(1), 100–109. doi:10.1016/j.conb.2010.09.004 [PubMed: 20889331]

Kim J, Sunagawa M, Kobayashi S, Shin T, & Takayama C (2016). Developmental localization of calcitonin gene-related peptide in dorsal sensory axons and ventral motor neurons of mouse cervical spinal cord. Neurosci Res, 105, 42–48. doi:10.1016/j.neures.2015.09.003 [PubMed: 26403381]

Kosaka Y, Kin H, Tatetsu M, Uema I, & Takayama C (2012). Distinct development of GABA system in the ventral and dorsal horns in the embryonic mouse spinal cord. Brain Res, 1486, 39–52. doi: 10.1016/j.brainres.2012.10.003 [PubMed: 23044470]

Lai HC, Seal RP, & Johnson JE (2016). Making sense out of spinal cord somatosensory development. Development, 143(19), 3434–3448. doi:10.1242/dev.139592 [PubMed: 27702783]

Larsson M (2017). Pax2 is persistently expressed by GABAergic neurons throughout the adult rat dorsal horn. Neurosci Lett, 638, 96–101. doi:10.1016/j.neulet.2016.12.015 [PubMed: 27939388]

Leggere JC, Saito Y, Darnell RB, Tessier-Lavigne M, Junge HJ, & Chen Z (2016). NOVA regulates Dcc alternative splicing during neuronal migration and axon guidance in the spinal cord. Elife, 5. doi:10.7554/eLife.14264

Li HSZZQ. (1998). Small sensory neurons in the rat dorsal root ganglia express functional NK-1 tachykinin receptor. European Journal of Neuroscience, 10, 1292–1299. [PubMed: 9749783]

Light AR (1988). Normal anatomy and physiology of the spinal cord dorsal horn. Appl Neurophysiol, 51(2–5), 78–88. [PubMed: 3291759]

Macias M, Dwornik A, Ziemlinska E, Fehr S, Schachner M, Czarkowska-Bauch J, & Skup M (2007). Locomotor exercise alters expression of pro-brain-derived neurotrophic factor, brain-derived neurotrophic factor and its receptor TrkB in the spinal cord of adult rats. Eur J Neurosci, 25(8), 2425–2444. doi:10.1111/j.1460-9568.2007.05498.x [PubMed: 17445239]

Madisen L, Zwingman TA, Sunkin SM, Oh SW, Zariwala HA, Gu H, … Zeng H (2010). A robust and high-throughput Cre reporting and characterization system for the whole mouse brain. Nat Neurosci, 13(1), 133–140. doi:10.1038/nn.2467 [PubMed: 20023653]

Marikawa Y, Fujita TC, & Alarcon VB (2004). An enhancer-trap LacZ transgene reveals a distinct expression pattern of Kinesin family 26B in mouse embryos. Dev Genes Evol, 214(2), 64–71. doi: 10.1007/s00427-003-0377-x [PubMed: 14727108]

Martinez E, & Tran TS (2015). Vertebrate spinal commissural neurons: a model system for studying axon guidance beyond the midline. Wiley Interdiscip Rev Dev Biol, 4(3), 283–297. doi:10.1002/wdev.173 [PubMed: 25619385]

Matise MP (2013). Molecular genetic control of cell patterning and fate determination in the developing ventral spinal cord. Wiley Interdiscip Rev Dev Biol, 2(3), 419–425. doi:10.1002/wdev.83 [PubMed: 23799585]

Melone M, Burette A, & Weinberg RJ (2005). Light microscopic identification and immunocytochemical characterization of glutamatergic synapses in brain sections. J Comp Neurol, 492(4), 495–509. doi:10.1002/cne.20743 [PubMed: 16228991]

Montag-Sallaz M, Schachner M, & Montag D (2002). Misguided Axonal Projections, Neural Cell Adhesion Molecule 180 mRNA Upregulation, and Altered Behavior in Mice Deficient for the Close Homolog of L1. Molecular and Cellular Biology, 22(22), 7967–7981. doi:10.1128/mcb.22.22.7967-7981.2002 [PubMed: 12391163]

Montana V, Ni Y, Sunjara V, Hua X, & Parpura V (2004). Vesicular glutamate transporter-dependent glutamate release from astrocytes. J Neurosci, 24(11), 2633–2642. doi:10.1523/JNEUROSCI.3770-03.2004 [PubMed: 15028755]

Mullen RJ, Buck CR, & Smith AM (1992). NeuN, a neuronal specific nuclear protein in vertebrates. Development, 116(1), 201–211. [PubMed: 1483388]

Neumann S, Braz JM, Skinner K, Llewellyn-Smith IJ, & Basbaum AI (2008). Innocuous, not noxious, input activates PKCgamma interneurons of the spinal dorsal horn via myelinated afferent fibers. J Neurosci, 28(32), 7936–7944. doi:10.1523/JNEUROSCI.1259-08.2008 [PubMed: 18685019]

Parra LM, & Zou Y (2010). Sonic hedgehog induces response of commissural axons to Semaphorin repulsion during midline crossing. Nat Neurosci, 13(1), 29–35. doi:10.1038/nn.2457 [PubMed: 19946319]

Patel Y (1999). Somatostatin and its receptor family. Front Neuroendocrinol, 20(3), 157–198. [PubMed: 10433861]

Petko M, Veress G, Vereb G, Storm-Mathisen J, & Antal M (2004). Commissural propriospinal connections between the lateral aspects of laminae III-IV in the lumbar spinal cord of rats. J Comp Neurol, 480(4), 364–377. doi:10.1002/cne.20356 [PubMed: 15558798]

Phelps PE, Alijani A, & Tran TS (1999). Ventrally located commissural neurons express the GABAergic phenotype in developing rat spinal cord. J Comp Neurol, 409(2), 285–298. [PubMed: 10379921]

Polgar E, Sardella TC, Watanabe M, & Todd AJ (2011). Quantitative study of NPY-expressing GABAergic neurons and axons in rat spinal dorsal horn. J Comp Neurol, 519(6), 1007–1023. doi: 10.1002/cne.22570 [PubMed: 21344400]

Ptak K, Burnet H, Blanchi B, Sieweke M, De Felipe C, Hunt SP, … Hilaire G (2002). The murine neurokinin NK1 receptor gene contributes to the adult hypoxic facilitation of ventilation. Eur J Neurosci, 16(12), 2245–2252. [PubMed: 12492418]

R.-Core-Team. (2017). R: A Language and Environment for Statistical Computing.

Ren K, & Ruda MA (1994). A comparative study of the calcium-binding proteins calbindin-D28K, calretinin, calmodulin and parvalbumin in the rat spinal cord. Brain Research Reviews, 19, 163–179. [PubMed: 8061685]

Renier N, Schonewille M, Giraudet F, Badura A, Tessier-Lavigne M, Avan P, … Chédotal A (2010). Genetic Dissection of the Function of Hindbrain Axonal Commissures. PLOS Biology, 8(3), e1000325. doi:10.1371/journal.pbio.1000325 [PubMed: 20231872]

Restrepo CE, Lundfald L, Szabo G, Erdelyi F, Zeilhofer HU, Glover JC, & Kiehn O (2009). Transmitter-phenotypes of commissural interneurons in the lumbar spinal cord of newborn mice. J Comp Neurol, 517(2), 177–192. doi:10.1002/cne.22144 [PubMed: 19731323]

Rexed B (1952). The cytoarchitectonic organization of the spinal cord in the cat. J Comp Neurol, 96(3), 414–495. [PubMed: 14946260]

Rodriguez CI, Buchholz F, Galloway J, Sequerra R, Kasper J, Ayala R, … Dymecki SM (2000). High-efficiency deleter mice show that FLPe is an alternative to Cre-loxP. Nat Genet, 25(2), 139–140. [PubMed: 10835623]

Ross SE, Mardinly AR, McCord AE, Zurawski J, Cohen S, Jung C, … Greenberg ME (2010). Loss of inhibitory interneurons in the dorsal spinal cord and elevated itch in Bhlhb5 mutant mice. Neuron, 65(6), 886–898. doi:10.1016/j.neuron.2010.02.025 [PubMed: 20346763]

Rousso DL, Gaber ZB, Wellik D, Morrisey EE, & Novitch BG (2008). Coordinated actions of the forkhead protein Foxp1 and Hox proteins in the columnar organization of spinal motor neurons. Neuron, 59(2), 226–240. doi:10.1016/j.neuron.2008.06.025 [PubMed: 18667151]

Sabatier CP,A; Ma; Brose; Tamada A; Murakami F; Lee E; Tessier-Lavigne MT. (2004). The Divergent Robo Family Protein Rig-1/Robo3 Is a Negative Regulator of Slit Responsiveness Required for Midline Crossing by Commissural Axons. Cell, 117, 157–169. [PubMed: 15084255]

Saito T, Iwata N, Tsubuki S, Takaki Y, Takano J, Huang SM, … Saido TC (2005). Somatostatin regulates brain amyloid beta peptide Abeta42 through modulation of proteolytic degradation. Nat Med, 11(4), 434–439. doi:10.1038/nm1206 [PubMed: 15778722]

Samad TA, Rebbapragada A, Bell E, Zhang Y, Sidis Y, Jeong SJ, … Woolf CJ (2005). DRAGON, a bone morphogenetic protein co-receptor. J Biol Chem, 280(14), 14122–14129. doi:10.1074/jbc.M410034200 [PubMed: 15671031]

Stokke MF, Nissen UV, Glover JC, & Kiehn O (2002). Projection patterns of commissural interneurons in the lumbar spinal cord of the neonatal rat. J Comp Neurol, 446(4), 349–359. [PubMed: 11954034]

Storm R, Cholewa-Waclaw J, Reuter K, Brohl D, Sieber M, Treier M, … Birchmeier C (2009). The bHLH transcription factor Olig3 marks the dorsal neuroepithelium of the hindbrain and is essential for the development of brainstem nuclei. Development, 136(2), 295–305. doi:10.1242/dev.027193 [PubMed: 19088088]

The UniProt Consortium. (2017). UniProt: the universal protein knowledgebase. Nucleic Acids Research, 45(D1), D158–D169. doi:10.1093/nar/gkw1099 [PubMed: 27899622]

Tiveron MC, Beurrier C, Ceni C, Andriambao N, Combes A, Koehl M, … Cremer H (2016). LAMP5 Fine-Tunes GABAergic Synaptic Transmission in Defined Circuits of the Mouse Brain. PLoS One, 11(6), e0157052. doi:10.1371/journal.pone.0157052 [PubMed: 27272053]

Todd AJ (2010). Neuronal circuitry for pain processing in the dorsal horn. Nat Rev Neurosci, 11(12), 823–836. doi:10.1038/nrn2947 [PubMed: 21068766]

Trapnell C, Roberts A, Goff L, Pertea G, Kim D, Kelley DR, … Pachter L (2012). Differential gene and transcript expression analysis of RNA-seq experiments with TopHat and Cufflinks. Nat Protoc, 7(3), 562–578. doi:10.1038/nprot.2012.016 [PubMed: 22383036]

Tsuchida T, Ensini M, Morton SB, Baldassare M, Edlund T, Jessell TM, & Pfaff SL (1994). Topographic organization of embryonic motor neurons defined by expression of LIM homeobox genes. Cell, 79(6), 957–970. [PubMed: 7528105]

Wang CH, Chen IH, Kuo MW, Su PT, Lai ZY, Wang CH, … Chuang YJ (2011). Zebrafish Thsd7a is a neural protein required for angiogenic patterning during development. Dev Dyn, 240(6), 1412–1421. doi:10.1002/dvdy.22641 [PubMed: 21520329]

Wilson SI, Shafer B, Lee KJ, & Dodd J (2008). A molecular program for contralateral trajectory: Rig-1 control by LIM homeodomain transcription factors. Neuron, 59(3), 413–424. doi:10.1016/j.neuron.2008.07.020 [PubMed: 18701067]

Wong T (2009). FoxP genes subdivide interneuron subclasses in the developing mouse spinal cord. (Master of Science), University of California San Diego, San Diego.

Xu Y, Lopes C, Qian Y, Liu Y, Cheng L, Goulding M, … Ma Q. (2008). Tlx1 and Tlx3 coordinate specification of dorsal horn pain-modulatory peptidergic neurons. J Neurosci, 28(15), 4037–4046. doi:10.1523/JNEUROSCI.4126-07.2008 [PubMed: 18400903]

Yamauchi K, Phan KD, & Butler SJ (2008). BMP type I receptor complexes have distinct activities mediating cell fate and axon guidance decisions. Development, 135(6), 1119–1128. doi:10.1242/dev.012989 [PubMed: 18272594]

Zelina P, Blockus H, Zagar Y, Peres A, Friocourt F, Wu Z, … Chedotal A (2014). Signaling switch of the axon guidance receptor Robo3 during vertebrate evolution. Neuron, 84(6), 1258–1272. doi:10.1016/j.neuron.2014.11.004 [PubMed: 25433640]

Zhang Y, Narayan S, Geiman E, Lanuza GM, Velasquez T, Shanks B, … Goulding M (2008). V3 spinal neurons establish a robust and balanced locomotor rhythm during walking. Neuron, 60(1), 84–96. doi:10.1016/j.neuron.2008.09.027 [PubMed: 18940590]

Zimmermann L, & Schwaller B (2002). Monoclonal antibodies recognizing epitopes of calretinins: dependence on Ca2+-binding status and differences in antigen accessibility in colon cancer cells. Cell Calcium, 31(1), 13–25. doi:10.1054/ceca.2001.0255 [PubMed: 11990296]

Zou Y, Stoeckli E, Chen H, & Tessier-Lavigne M (2000). Squeezing Axons Out of the Gray Matter- A Role for Slit and Semaphorin Proteins from Midline and Ventral Spinal Cord. Cell, 102, 363–375. [PubMed: 10975526]

Tulloch AJ, Teo S, Carvajal BV, Tessier-Lavigne M, Jaworski A; 2019; Transcriptomic analysis of embryonic commissural neurons; Figshare; 10.6084/m9.figshare.8023436

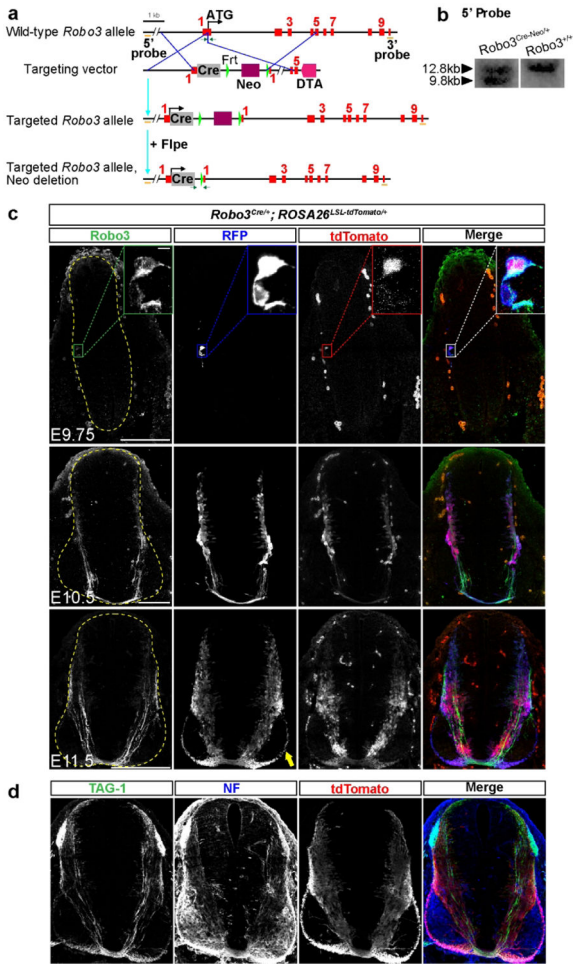

Figure 1. Cre expression from the *Robo3* locus recapitulates Robo3 expression in spinal commissural neurons during development.

(**a**) A schematic of the targeting strategy to insert *Cre* into the *Robo3* locus. The *Cre* coding sequence replaces the first 34 nucleotides of the *Robo3* coding sequence in exon 1. Southern blot probes (orange lines) and PCR primers (green arrows) for genotyping are indicated. (**b**) Southern blot analysis of *SspI*-digested genomic DNA with a probe located upstream of the 5' homology arm. Targeted ES cell clones are identified by a knock-in fragment at 9.8 kb and a WT fragment at 12.8 kb. (**c, d**) Transverse sections of *Robo3*$^{Cre/+}$; *ROSA26*$^{LSL\text{-}tdTomato/+}$ spinal cords at the indicated ages were labeled with antibodies against Robo3 and RFP or TAG-1 and NF. RFP staining and tdTomato fluorescence label Robo3^{+} neurons and their axons (**c**), including postcrossing C-axons (arrow); dashed outline marks spinal cord, inset shows magnified view of a single labeled neuron (boxed area). TAG-1 and NF staining confirms that tdT^{+} cells are C- neurons (**d**). Scale bars: 100 μm in **c** top row; 5 μm in **c** top row insets; 100 μm in **c** middle row; 250 μm in **c** bottom row and **d**.

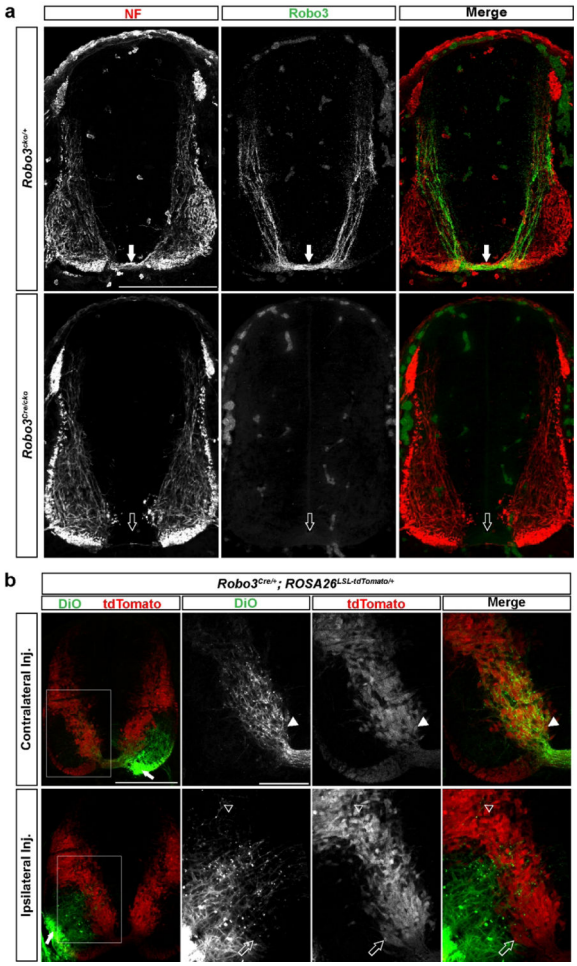

Figure 2. *Robo3*^{Cre} provides genetic access to commissural neurons.

(**a**) Labeling of E11.5 *Robo3*$^{cko/+}$ (top) or *Robo3*$^{Cre/cko}$ (bottom) spinal cord sections for NF and Robo3 reveals absence of the ventral commissure in *Robo3*$^{Cre/cko}$ embryos (empty arrow), but not *Robo3*$^{cko/+}$ littermate control (arrow), and shows no detectable Robo3 protein in *Robo3*$^{Cre/cko}$ embryos. (**b**) DiO was injected (arrow) directly adjacent to the ventral commissure (top) or into the lateral funiculus (bottom) of transverse spinal cord sections from E11.5 *Robo3*$^{Cre/+}$; *ROSA26*$^{LSL\text{-}tdTomato/+}$ mice. Boxed regions in left column indicate magnified areas shown in other panels. All retrogradely traced DiO^{+} neurons contralateral to the injection site are tdT^{+} (arrowhead), and tdT^{+} neurons ipsilateral to the injection site are DiO^{-} (empty arrow); empty arrowhead indicates DiO^{+} ipsilateral neuron that does not express tdTomato. Scale bars: 250 μm in **a** and **b** low magnification images; 100 μm in **b** high magnification images.

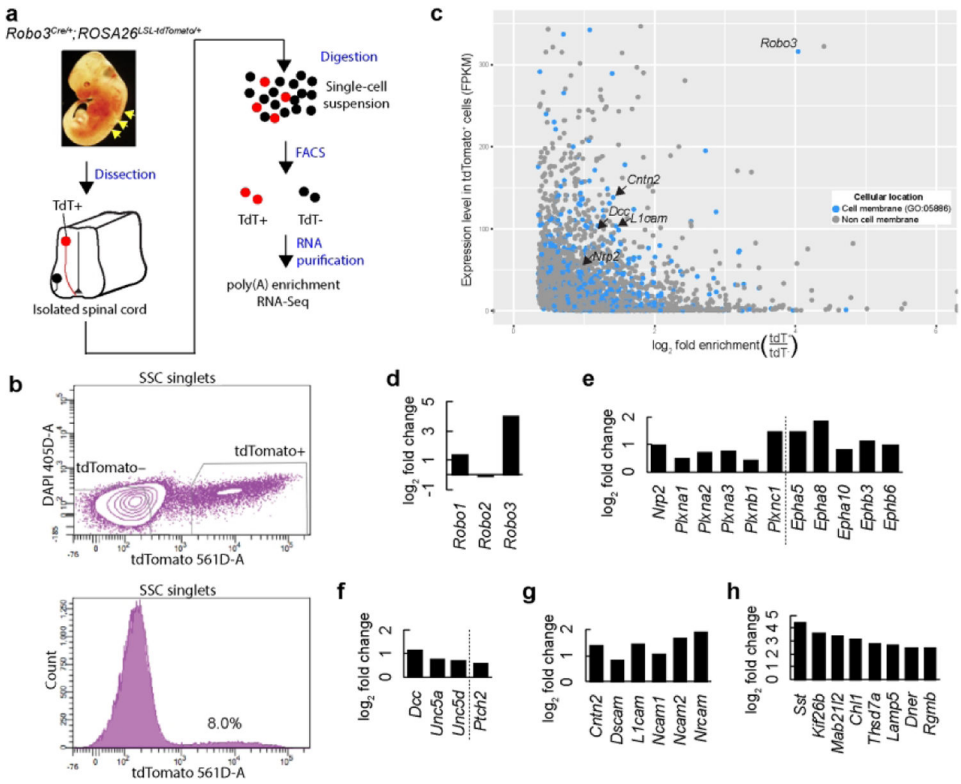

Figure 3. RNA-Seq analysis identifies mRNAs enriched in E11.5 commissural neurons.

(**a**) Flowchart of RNA-Seq analysis after FACS of dissociated E11.5 *Robo3*$^{Cre/+}$; *ROSA26*$^{LSL\text{-}tdTomato/+}$ spinal cords. Yellow arrows indicate the location along the rostro-caudal axis of the developing spinal cord that was dissected and isolated from the rest of the embryo. (**b**) Top: a representative FACS density plot showing how tdT^{+} neurons were enriched from *Robo3*$^{Cre/+}$; *ROSA26*$^{LSL\text{-}tdTomato/+}$ embryos (n=11 embryos). Quadrilaterals indicate gates to segregate tdT^{+} and tdT^{-} populations. Bottom: a representative histogram of cells from the same experiment. Approximately 8% of sorted cells were tdT^{+}. (**c**) Levels of mRNAs that were enriched (cutoff: $q < 0.05$) in tdT^{+} neurons (measured in fragments per kb gene per million reads (FPKM)) were plotted against their enrichment compared to tdT^{-} cells ($\log_2$ scale). Select genes commonly associated with C-neurons are labeled. (**d-h**) Relative expression levels of select mRNAs in C-neurons. Enrichments factors ($\log_2$ scale) are shown for Robo family members (**d**), enriched guidance receptors for Semaphorins or Ephrins (separated by dashed line) (**e**), preferentially expressed receptors for Netrin-1 or Shh (separated by dashed line) (**f**), enriched cell adhesion molecules (**g**), and highly expressed and enriched mRNAs that were selected for further investigation via *in situ* hybridization (**h**).

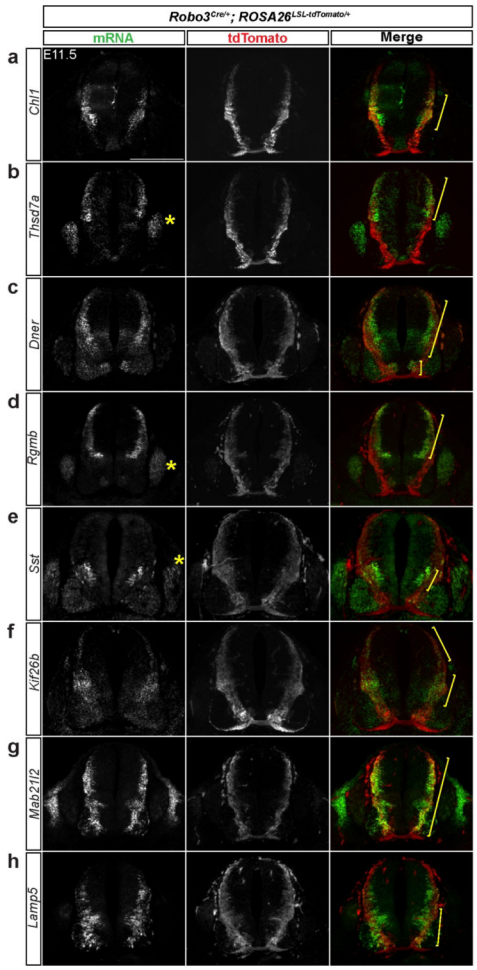

Figure 4. Expression validation of select transcripts enriched in commissural neurons by *in situ* hybridization.

(**a-h**) E11.5 *Robo3*$^{Cre/+}$; *ROSA26*$^{LSL\text{-}tdTomato/+}$ transverse spinal cord sections were analyzed by fluorescent *in situ* hybridization for mRNAs that were highly expressed and enriched in C-neurons. *Chl1* (**a**), *Thsd7a* (**b**), *Dner* (**c**), *Rgmb* (**d**), *Sst* (**e**), *Kif26b* (**f**), *Mab21l2* (**g**), and *Lamp5* (**h**) exhibit strong expression in subsets of tdT^{+} C-neurons, with some mRNAs being also detected in other spinal cord neurons. Brackets indicate regions of co-localization between tdTomato signal and mRNA expression, and asterisks mark mRNA expression in DRGs. Scale bar: 250 μm.

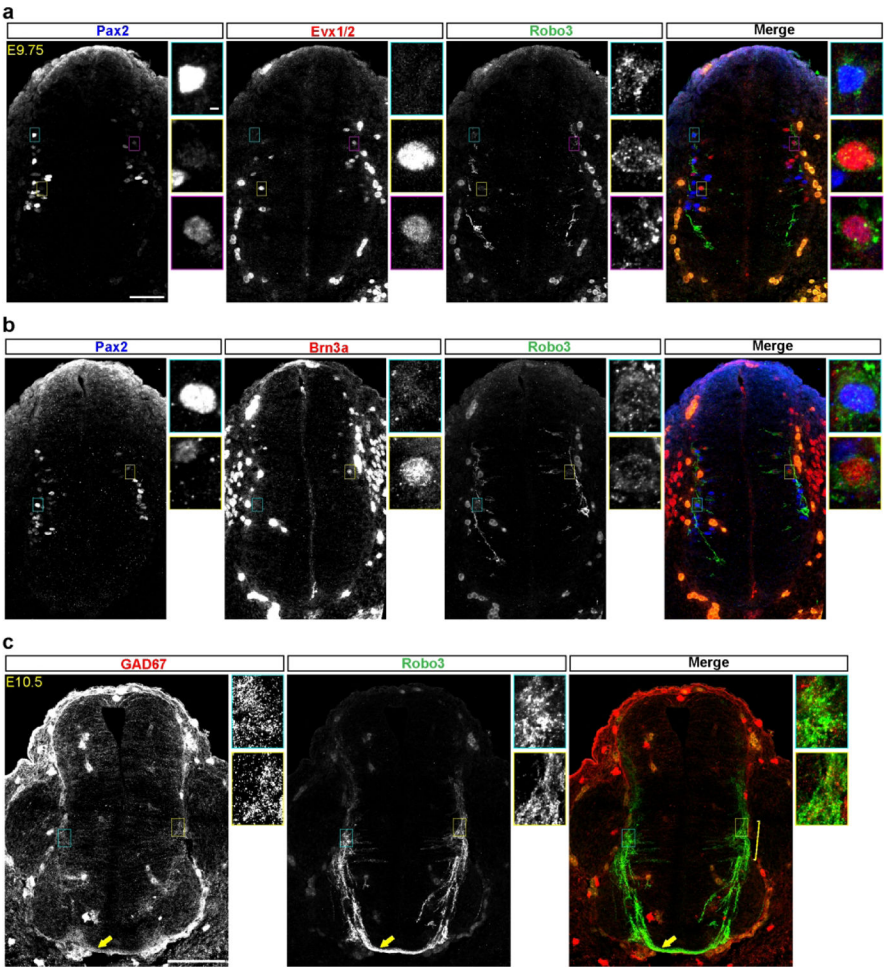

Figure 5. DI4-V0 C-neurons send pioneer axons towards the midline.

(**a,b**) Transverse spinal cord sections from E9.75 embryos were labeled with antibodies against Evx1/2 or Brn3a, as well as Robo3 and Pax2. The first Robo3-expressing C-neurons that project axons towards the midline are located in the intermediate spinal cord and belong to the dI4 or dI6 subtypes ($Pax2^+/Evx1/2^-$, (blue box, also shown at higher magnification)), the $V0_V$ class ($Pax2^-$ /$Evx1/2^+$ (yellow box)), and the $V0_D$, $V0_C$, or $V0_G$ subtypes ($Pax2^+$/$Evx1/2^+$ (magenta box)) (**a**). Early Robo3-expressing neurons also fall into the dI5 class ($Brn3a^+/Pax2^-$ (yellow box)), mutually exclusive from dI4/dI6/V0 C-neurons ($Pax2^+/Brn3a^-$ (blue box)) (**b**). (**c**) Staining of transverse E10.5 spinal cord sections with antibodies against Robo3 and GAD67 shows GAD67 expression in some $Robo3^+$ cells in the intermediate spinal cord (insets and bracket) and some (arrow) $Robo3^+$ axons in the commissure. Scale bars: 50 μm in **a** and **b** low magnification images; 100μm in **c** low magnification images; 5 μm in insets.

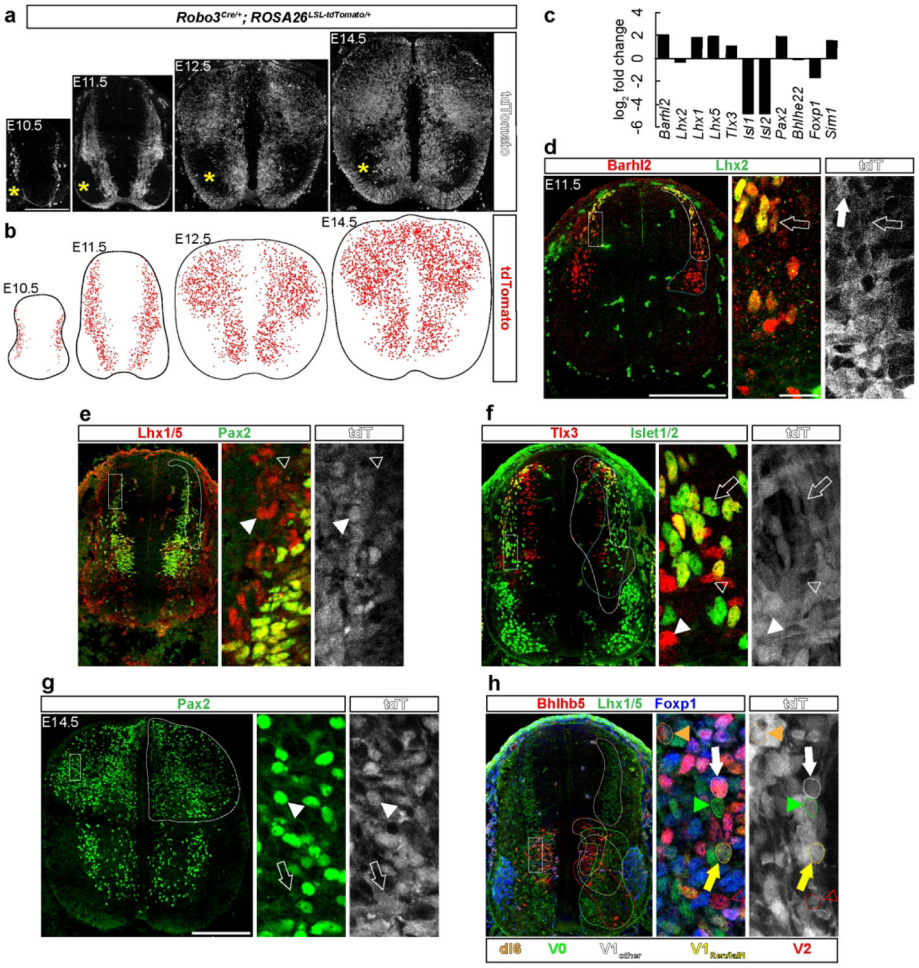

Figure 6. Analysis of commissural neuron subtypes during development.

(**a**) Representative transverse sections of E10.5, E11.5, E12.5, and E14.5 *Robo3*$^{Cre/+}$; *ROSA26*$^{LSL\text{-}tdTomato/+}$ spinal cords show localization of tdT^{+} C-neurons in most areas of the spinal cord except the ventral horn (asterisk). (**b**) Schematic diagrams of the average distribution of tdTomato- labeled C-neurons in transverse sections of E10.5, E11.5, E12.5, and E14.5 spinal cords (n=3 embryos). (**c**) Relative expression levels of mRNAs that are specific for subtypes of spinal cord neurons. Enrichments factors ($\log_2$ scale) of indicated transcription factors in C-neurons are derived from RNA-Seq analysis of tdT^{+} and tdT^{-} cells (see Figure 2). (**d-h**) Transverse E10.5, E11.5, E12.5, and E14.5 *Robo3*$^{Cre/+}$; *ROSA26*$^{LSL\text{-}tdTomato/+}$ spinal cord sections were stained with antibodies against combinations of transcription factors analyzed in **c** to label different neuronal classes. Shown are E11.5 and E14.5 examples, and regions within the white boxes (left panels) are also displayed at higher magnification (middle and right panels). Stainings for Lhx2 and Barhl2 (**d**), Pax2 and Lhx1/5 (**e**), Isl1/2 and Tlx3 (**f**), Pax2 (**g**), and Lhx1/5, Bhlhb5, and Foxp1 (**h**) were combined with positional criteria to identify dI1 (**d**), dI2 (**e**), dI3 (**f**), dI4 (**e,g**), dI5 (**f**), dI6 (**h**), V0 (**h**), $V1_{other}$ (**h**), $V1_{Ren/IaIN}$ (**h**), and V2 neurons (**h**) (see Materials and Methods for details). Dashed outlines indicate regions where neuronal populations reside: Barhl2^{+}/Lhx2^{+} (white) and Barhl2^{+}/Lhx2^{-} (blue) neurons (**d**), dI2 neurons (**e**), dI3 (white) and dI5

(light blue) (**f**), dI4/dIL$_A$ neurons (**g**), and dI6 (light orange), V0 (green), V1$_{other}$ (white), V1$_{Ren/IaIN}$ (yellow), and V2 (red) neurons (**h**). White arrowheads in **d-g** highlight tdT$^+$ (filled) or tdT$^-$ (empty) neurons from the Barhl2$^+$/Lhx2$^-$ (**d**), dI2 (**e**), dI5 (**f**), and dI4/dIL$_A$ (**g**) populations. White arrows in **d** identify tdT$^+$ (filled) or tdT$^-$ neurons (empty) from the Barhl2$^+$/Lhx2$^+$ population. Empty white arrow in **f** identifies a tdT$^-$ neuron from the dI3 population. Empty white arrow in **g** shows a tdT$^+$ C-neuron that does not express Pax2 (**g**). Filled arrows and arrowheads in **h** highlight tdT$^+$ C-neurons belonging to the dI6, V0, V1$_{other}$, and V1$_{Ren/IaIN}$ (see bottom key) populations. V2 neurons do not express tdTomato (empty red arrowhead). Scale bars: 250 μm in **a**; 250 μm in **d-f** and **h** low magnification images; 20 μm in **d-h** high magnification images; 250 μm in **g** low magnification image.

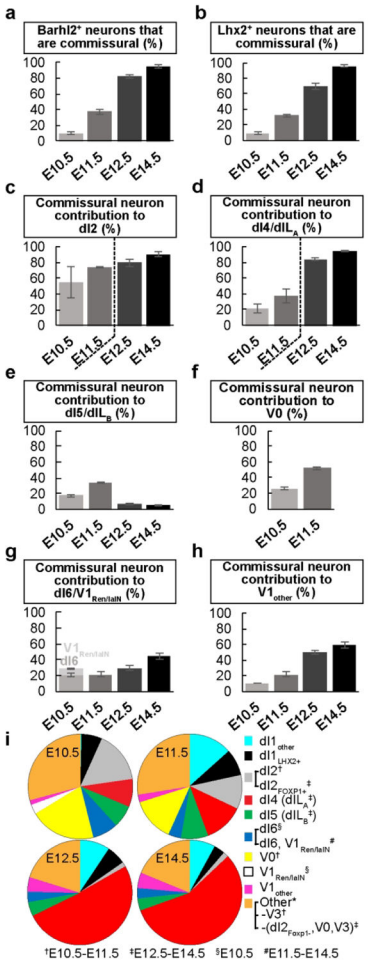

Figure 7. Quantification of commissural neuron subtypes during development.

Quantification of C-neuron contributions to different neuronal subtypes at E10.5, E11.5, E12.5, and E14.5: dI1 (**a, b**), dI2 (**c**), dI4/dIL$_A$ (**d**), dI5/dIL$_B$ (**e**), V0 (**f**), dI6/V1$_{Ren/IaIN}$ (**g**), and V1$_{other}$ (**h**) (n=3 embryos per age). Values in **c, d** were derived from different antibody labeling combinations at E10.5/E11.5 and E12.5/E14.5 (separated by dashed line; see Materials and Methods). E12.5 and E14.5 values in **f** are absent due to loss of detectable Lhx1/5 expression. In **g**, the dI6 and V1$_{Ren/IaIN}$ populations could be separated by position at E10.5 only. (**i**) Pie charts showing quantitative contribution of different spinal cord neuron subtypes to the entire C-neuron population at E10.5, E11.5, E12.5, and E14.5. Key (right) corresponds to the respective neuronal classes that contain C-neurons at all ages, unless indicated otherwise. “Other” encompasses all neurons that contribute to the C-neuron population and could not be categorized by the applied criteria. Error bars indicate SEM.

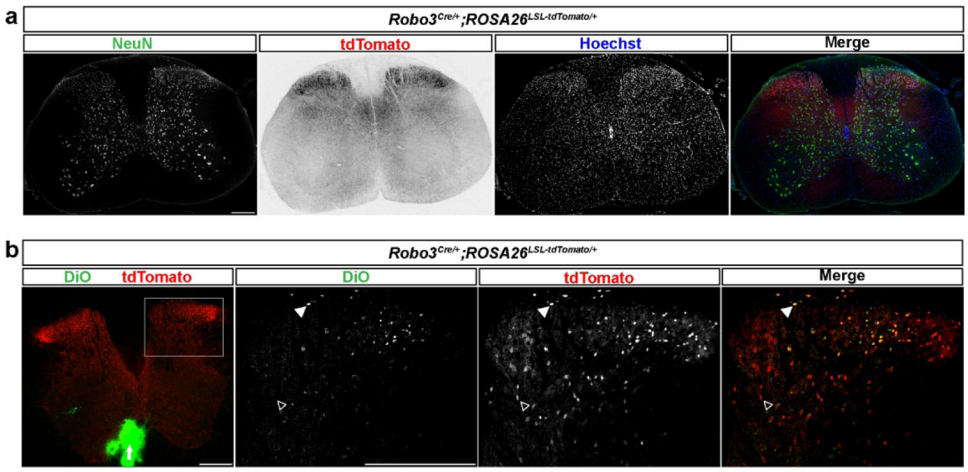

Figure 8. Labeling of commissural neurons in adult *Robo3*$^{Cre/+}$; *ROSA26*$^{LSL\text{-}tdTomato/+}$ spinal cords.

(**a**) Transverse sections of adult *Robo3*$^{Cre/+}$; *ROSA26*$^{LSL\text{-}tdTomato/+}$ spinal cords were labeled with nuclear Hoechst stain and with antibodies against NeuN to visualize all cells and neurons, respectively. TdT^{+} cells are exclusively neuronal. (**b**) DiO was injected (arrow) directly adjacent to the ventral commissure in transverse spinal cord sections from adult *Robo3*$^{Cre/+}$; *ROSA26*$^{LSL\text{-}tdTomato/+}$ mice. Boxed area in left image indicates magnified region shown in other panels. All DiO^{+} cells contralateral to the injections site are tdT^{+} (arrowhead); empty arrowhead indicates a tdT^{+} neuron contralateral to the injection site that is DiO^{-}. Scale bars: 250 μm in **a**; 250 μm in **b** low magnification image; 250 μm in **b** high magnification images.

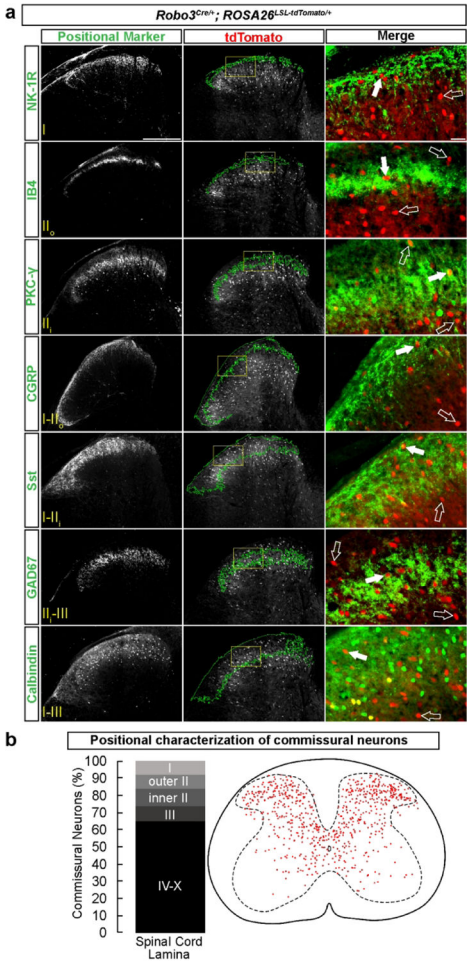

Figure 9. Mature commissural neurons are localized throughout the spinal cord gray matter.

(**a**) Transverse sections of adult *Robo3*$^{Cre/+}$*; ROSA26*$^{LSL\text{-}tdTomato/+}$ spinal cords were stained for markers specific to one or several lamina(e). Images show dorsal horn only. Left column: markers identifying laminae – NK-1R (lamina I), IB4 (outer lamina II (II_o)), PKC-γ (inner lamina II (II_{inner})), CGRP (I-II_{outer}), Sst (I-II_{inner}), GAD67 (II_{inner}-III), and CB (I-III). Middle: tdTomato labeling in the dorsal horn overlaid with intensity-based ROIs (green) created from lamina markers. Right: enlarged (from yellow boxes in middle) and merged marker and tdTomato labeling. TdT^+ C- neurons residing within or outside of the respective lamina(e) are indicated with filled or empty arrows, respectively. (**b**) Quantification of C-neurons in different spinal cord laminae (n=5 mice) and a schematic diagram of the average distribution of C-neurons in transverse sections of adult spinal cord (n=4 mice). Dashed outline indicates gray matter. Scale bars: 250 μm in **a** low magnification images; 20 μm in **a** high magnification images.

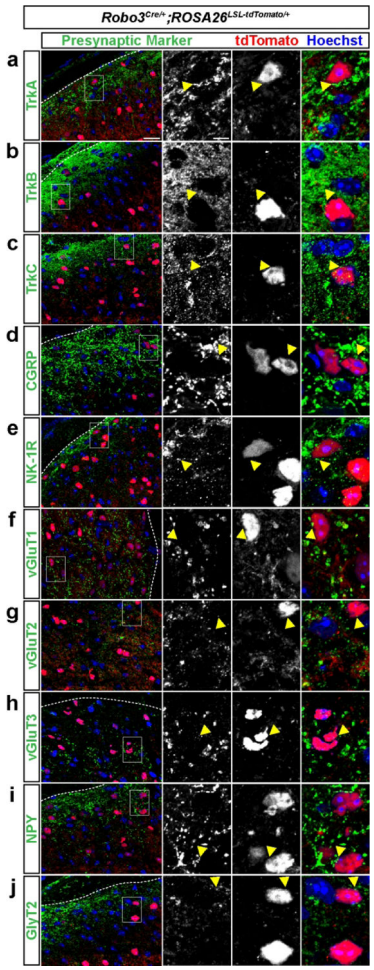

Figure 10. Commissural neurons in the adult spinal cord receive a diverse array of presynaptic inputs.

(**a-j**) Transverse sections of adult *Robo3*$^{Cre/+}$; *ROSA26*$^{LSL\text{-}tdTomato/+}$ spinal cords were stained with Hoechst dye and antibodies against markers for populations of sensory axons or different types of presynaptic terminals. TrkA^{+} (**a**), TrkB^{+} (**b**), TrkC^{+} (**c**), CGRP^{+} (**d**), NK-1R^{+} (**e**), vGluT1^{+} (**f**), vGluT2^{+} (**g**), vGluT3^{+} (**h**), NPY^{+} (**i**), and GlyT2^{+} (**j**) nerve terminals are found in close apposition (yellow arrowheads) with tdT^{+} C-neuron cell bodies. Magnified regions in columns 2–4 are indicated by white boxes in the first column. Dashed white lines in the left column indicate border of the spinal cord gray matter. Scale bars: 20 μm in **a-j** low magnification images; 5 μm in **a-j** high magnification images.

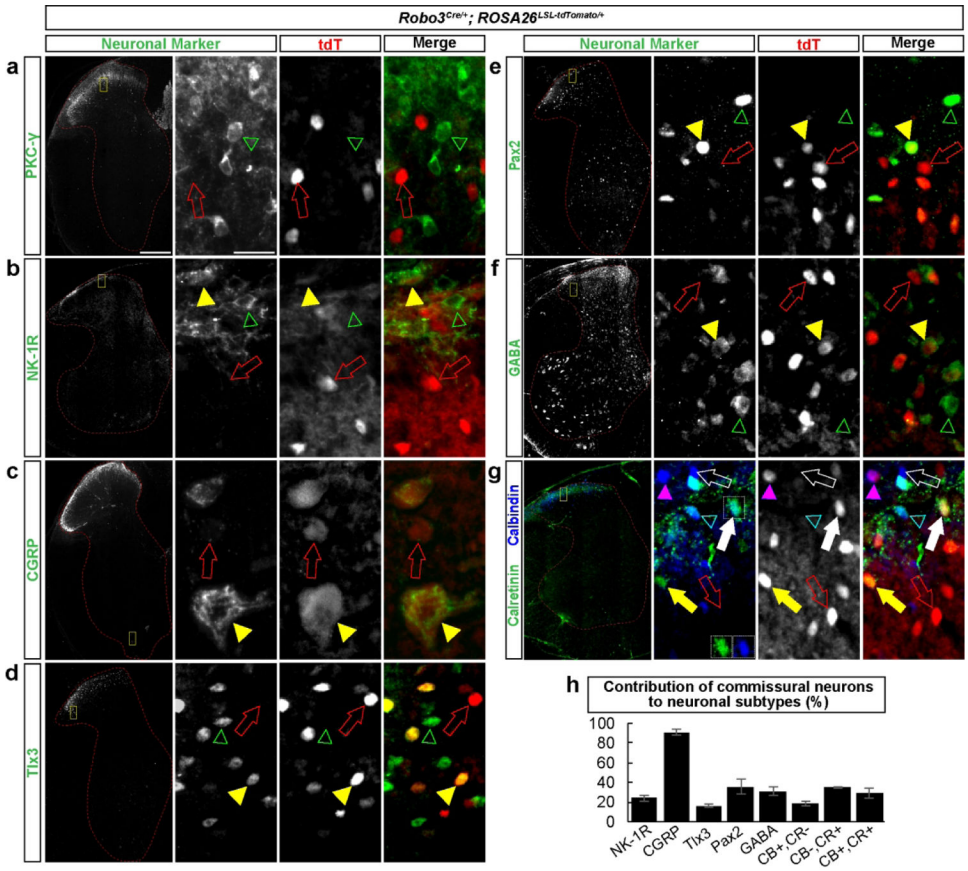

Figure 11. Mature commissural neurons exhibit molecular heterogeneity.

(**a-g**) Transverse sections of adult *Robo3*$^{Cre/+}$; *ROSA26*$^{LSL\text{-}tdTomato/+}$ spinal cords were stained with antibodies that mark neuronal subtypes. Shown are hemisections (first column; dashed red outline indicates gray matter) and enlarged regions (from yellow boxes; columns 2–4) labeled for PKC-γ (**a**), NK-1R (**b**), CGRP (**c**), Tlx3 (**d**), Pax2 (**e**), GABA (**f**), and CB plus CR (**g**). In some neurons, neuronal markers and tdTomato (tdT) are co-expressed (yellow arrowheads), while others are only positive for either the neuronal marker (empty green arrowhead) or tdTomato (empty red arrow). In **g,** neurons may be CR$^+$/CB$^+$/tdT$^+$ (white arrow), CR$^+$/CB$^+$/tdT$^-$ (empty cyan arrowhead), CR$^-$/CB$^+$/tdT$^+$ (purple arrowhead), CR$^-$/CB$^+$/tdT$^-$ (empty white arrow), or CR$^+$/CB$^-$/tdT$^+$ (yellow arrow). Inset in **g** shows separated CB and CR channels from the representative CB$^+$/CR$^+$/tdT$^+$ neuron. (**h**) Quantification of tdT$^+$ C-neuron contribution to each neuronal subtype (n=3 mice). Scale bars: 250 μm in **a-g** low magnification images; 20 μm in **a-g** high magnification images. Error bars indicate SEM.

Table 1.

Primers used to generate *in situ* probes

Gene	Forward primer	Reverse primer
Sst	ggagacgctaccgaagccgtcgctgctgc	cataatctcaccataattttattttgtat
Dner	tgactcccattgcctacgaggattacagt	cctcgacctgctaacgtttattcaatatt
Lamp5	cgcctacacactcagaatgctctttgtaa	caagacatgccttccatccctgggtttaa
Rgmb	tgaggtccttccgatccacgcacgtcga	ggtgcctatgtagcgggcatgcatctcta
Thsd7a	agaattttgttggattgtcccaggaaaag	gcaaggattttagttttagtcttcctttg
Chl1	cctttgccccagtgatccagctttaggag	actggatatgtggagttggtaggccctcc
Mab21l2	gcaaacctcagagtgcgctgcggcctga	gatcttgcgcgcagaaaggtagccagacg
Kif26b	ttggggaaccattcgaaattaaagtctatg	gacagttaacatttattcagctgcaatacc

All sequences are listed from 5’ to 3’.

Table 2.

Markers used for identification of neuronal classes in embryonic spinal cords.

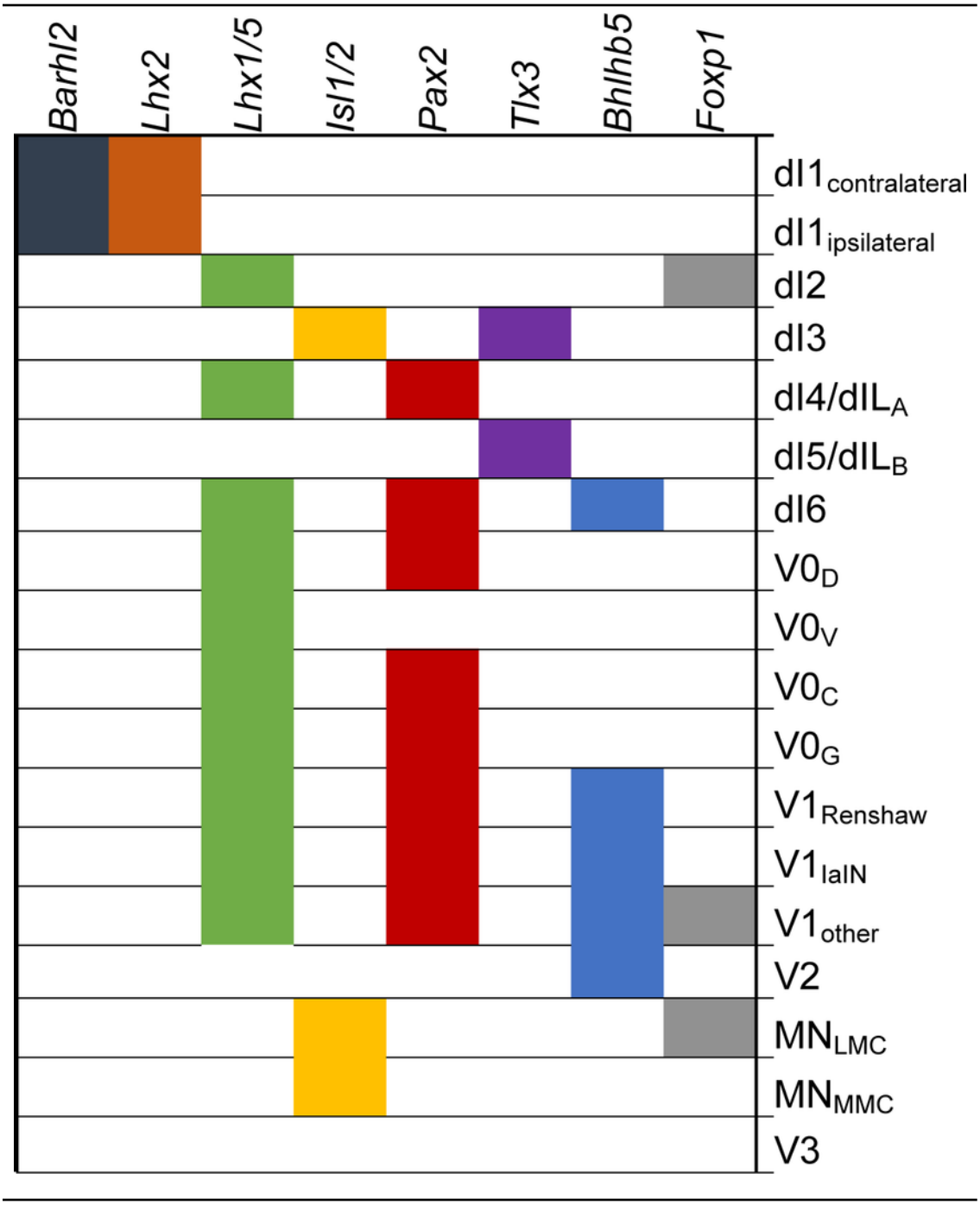

Abbreviations: D, Dorsal; V, Ventral; C, Cholinergic; G, Glycinergic; IaIN, Inhibitory Ia fiber; LMC, lateral motor column; MMC, medial motor column

Table 3.

Quantitative contribution of spinal cord neuron subtypes to the entire commissural neuron population.

Neuronal Class	Percent of C-neuron population			
	E10.5	E11.5	E12.5	E14.5
dI1 ($Lhx2^+$)	6.38±0.74	8.21±0.66	5.97±1.61	3.40±0.54
dI1 ($Barhl2^+/Lhx2^-$)	0.37±0.02	13.37±1.13	9.38±1.66	7.95±0.82
dI2	15.98±3.93	10.46±0.11	1.42±0.26t	1.61±0.08†
$dI4/dIL_A$	8.60±1.26	12.32±0.67	51.01±1.38	56.54±0.84
$dI5/dIL_B$	6.89±1.82	8.41±0.27	4.30±0.33	3.74±0.15
dI6	7.90±1.16	3.95±0.60	3.22±0.13	3.18±0.17
$V1_{Ren/IaIN}$	3.12±0.27			
V0	20.19±0.26	13.40±0.23	NA	NA
$V1_{other}$	1.43±0.57	2.34±0.45	4.51±0.16	4.79±0.31
Other‡	29.14	27.54	20.19	18.79

†$Foxp1^+$ subset of dI2 neurons

‡Remaining C-neurons do not fall under any of the defined neuronal classes and are likely a mix of V3 neurons and, at E12.5 and E14.5, $Foxp1^-$ dI2 neurons and V0 neurons